GEOLOGICAL SURVEY OF CANADA
OPEN FILE 7516

Variability of coastal change along the western Yukon coast

A.M. Konopczak, G.K. Manson, N.J. Couture

2014

Natural Resources Canada | Ressources naturelles Canada

Canada

GEOLOGICAL SURVEY OF CANADA
OPEN FILE 7516

Variability of coastal change along the western Yukon coast

A.M. Konopczak[1,2]
G.K. Manson[2,3]
N.J. Couture[2]

[1] Department for Geography, Christian-Albrechts-Universität zu Kiel, Kiel, Germany
[2] Geological Survey of Canada - Atlantic, Bedford Institute of Oceanography, Dartmouth, Nova Scotia
[3] Department of Geography, University of Guelph, Guelph, Ontario

2014

©Her Majesty the Queen in Right of Canada 2014

doi:10.4095/293788

This publication is available for free download through GEOSCAN (http://geoscan.ess.nrcan.gc.ca/).

Recommended citation
Konopczak, A.M., Manson, G.K., and Couture, N.J., 2014. Variability of coastal change along the western Yukon coast; Geological Survey of Canada, Open File 7516, 81 p. doi:10.4095/293788

Publications in this series have not been edited; they are released as submitted by the author.
Cover photo: Komakuk Beach, Konopczak (2012).

Table of Contents

Abstract 1

Introduction 2
Aims and Objectives 6

Study Area 6
Geology and Geomorphology 7
Arctic coastal processes 8
Thermal abrasion 8
Thermal denudation 9
Sea ice processes 10
Vegetation 11
Climate 11
Sea ice 11
Water levels 11
Storms 11
Study site descriptions 12
Border site 12
Komakuk Distant Early Warning Line Station 13
Komakuk site description 13
The coast between the Komakuk and Border sites 15

Data and Methods 17
Field survey data 17
Data acquisition 18
Data preparation 20
Data processing 21
Remote sensing data 23
Data acquisition 23
Data preparation 24
Functionality of the DSAS tool 26
Data processing 26
DSAS statistics 28
Calculation of total land loss 29

Results 30
GPS surveys 30
Border site erosion rates 30
Border site shore profiles 32
Komakuk site erosion rates 34
Komakuk site shore profiles 38
DSAS analysis 40
DSAS results of complete time series 41
DSAS results for time period analysis for the entire study area 44
DSAS results for time period analysis for the Border site 45
DSAS results for time period analysis for the Komakuk site 47
Calculation of total land loss 49

Discussion **49**
Variability of erosion **49**
Entire study area *49*
Border site *50*
Komakuk site *51*
Evaluation of methodology **51**
Correlations of shore profile parameters with erosion **52**

Conclusions **54**

Acknowledgements **54**

References **55**

Appendices **62**

Variability of coastal change along the western Yukon coast

A. M. Konopczak[1,2], G.K. Manson[2,3], N. J. Couture[2]
[1] Department for Geography, Christian-Albrechts-Universität zu Kiel, Kiel, Germany
[2] Geological Survey of Canada - Atlantic, Bedford Institute of Oceanography, Dartmouth, NS
[3] Department of Geography, University of Guelph, Guelph, ON

Abstract

Because the Yukon coast along the Beaufort Sea has the highest ground ice contents in the Canadian Arctic and, in addition, faces the direction of most effective storms, this section of coast is considered to be highly vulnerable to the effects of climate change. In order to gain insight into the regional coastal dynamics, a quantification of coastal change was undertaken that allowed the determination of spatial and temporal variability of coastal change along a 35 km long section of coast, stretching from Komakuk to the international border. Shorelines from several years between 1951 and 2009 were digitized from georeferenced aerial photographs and an ortho-rectified SPOT image. Shoreline change statistics were subsequently calculated using the Digital Shoreline Analysis System (DSAS) extension for Esri ArcGIS. Theodolite and real-time kinematic GPS data that was collected during several surveys between 1991 and 2012 at two Geological Survey of Canada (GSC) monitoring sites (Border site and Komakuk site) were analysed to provide higher temporal resolution of coastal change for the last two decades. Additionally, the field survey data enabled an assessment to be made of the contribution of geomorphic variables (i.e. beach slope, beach width, cliff slope, absolute cliff height, relative cliff height) towards explaining changes of coastal erosion.

According to the findings, the mean annual erosion along the western Yukon coast has been -1.2 ± 0.4 m/a over the entire period of study, with the rates decreasing through time from -1.4 ± 0.6 m/a between 1951 and 1972, to -1.2 ± 0.5 m/a between 1972 and 2009. However, site specific investigations show that there are differences in the mean erosion rates and in temporal trends. To the west at the Border site, the mean annual erosion rate is -1.3 ± 0.3 m/a, and the rates have recently accelerated, while at Komakuk in the east of the study area, the mean annual erosion rate is -0.9 ± 0.2 m/a, with the rates decelerating over time. A comparison of these findings to erosion rates from the Alaskan Beaufort Sea coast indicates that there is a general spatial pattern of decreasing erosion rates from the west to the east. The quantified erosion rates also enabled the calculation of mean annual land loss between 1951 and 2009, which amounted to 4.5 ha/a. An analysis of the influence of shore profile parameters on mean annual erosion rates showed a statistically significant correlation between beach widths and erosion rates (r=0.84) at the Border site. There is also a strong but insignificant correlation between absolute cliff heights and erosion rates at the Border, but no correlations of shore profile parameters with erosion could be distinguished for the Komakuk site.

Introduction

The Arctic is a sparsely populated region primarily known for its harsh and cold climate during long winters. In the last decade, in particular, this remote region has been attracting more and more attention, as an important region in terms of global climate change. Observations of the Earth's climate indicate a global rise in temperature in response to increasing concentrations of greenhouse gases (Treut et al. 2007). This trend is amplified in the Arctic (Johannessen et al. 2004). While prognoses from the Intergovernmental Panel on Climate Change (IPCC) forecast an increase of global increase of global mean surface air temperatures of 1.7 °C to 4.4 °C by 2099 (A1B scenario) (Meehl et al. 2007), projections for the Arctic show a 3 °C to 6 °C warming of surface air temperature by 2080 (AMAP 2012). These different prognoses result from a regional feedback phenomenon known as arctic amplification. Rising surface air temperatures lead to a diminution of both land and sea ice and a decrease in the extent of these highly reflective surfaces resulting in a lowering of ice-albedo and therefore an increase in the absorption of solar radiation. Subsequent further warming and reduction of the albedo of the sea ice and land surfaces leads to an intensification of the process. Consequently, the described ice-albedo feedback leads to an amplification of the initial temperature change (Holland et al. 2006; Serreze & Francis 2006; Anisimov et al. 2007; AMAP 2012).

Evidence of this process is given by numerous investigations focusing on changing sea ice extents, soil temperatures, air temperatures and precipitation patterns, all of which indicate a rapid acceleration of change within the last four decades (Serreze et al. 2000). For example in 2012, sea ice extent fell to an overall minimum of just 3.41 million km², down from the long-term average of 6.71 million km² and below the record minimums reached in 2007 and 2002 (Perovich et al. 2012). Soil temperatures have increased on average of 2 °C within the last several decades, and the increase in average air temperature since 1980 has been twice as high in the Arctic as it was in the rest of the world (IPCC 2007; AMAP 2012; Romanovsky et al. 2012). As mentioned above, projections forecast a temperature increase of 3 to 6 °C by 2080 (AMAP 2012), and the possibility of a nearly ice free Arctic basin by 2040 (Holland et al. 2006). Since polar regions are considered to have the great potential for affecting global climate (Rachold et al. 2004; Anisimov et al. 2007), their detailed investigation is of major importance.

Changes in Arctic climate conditions trigger a number of environmental responses. For the purpose of this work, the most important responses to Arctic climate changes are changes of factors that lead to the acceleration of coastal erosion. In particular, these are:

- An increase in the thawing depth of the soil, as this prompts landscape degradation and facilitates erosion (Serreze et al. 2000; Jorgenson & Brown 2005; Dupeyrat et al. 2011).
- An extended open water season, as this reduces the time in which the shore is protected from coastal erosion by sea ice (Atkinson 2005).
- A decrease of the summer sea ice extent, as open water fetch gets longer allowing the generation of higher waves (Couture 2010, after McGillvray 1993).
- An increase in the number of severe storms, as storms are the most effective erosive agents (Lambert 1995; Aré et al. 2008).
- An increase in sea water temperature, as this accelerates the thermal and mechanical erosion of frozen sediments (Kobayashi et al. 1999).
- A relative sea level rise, as a higher sea level allows larger and thus more powerful waves to approach closer to the shore (Manson & Solomon 2007; Bird 2009).

Since the majority of the world's population lives within a short distance of the sea, coastal erosion is a major and well-known threat resulting from climate change. The Arctic is no exception, with most communities and cultural sites situated right next to the ocean; consequently, they are highly vulnerable to coastal erosion, even though the Arctic Ocean remains frozen for about nine months each year, which inhibits wave generation (Atkinson 2005). Despite the fact that most of the coastal erosion only occurs during the short open water season, arctic coasts nevertheless have the highest erosion rates in the world, by far (Reimnitz et al. 1988; Reimnitz & Aré 1998).

Approximately 50% of the global soil organic carbon is stored in the perennially frozen ground of the Arctic (Tarnocai et al. 2009), so coastal erosion also alters carbon distribution by transferring soil carbon to the ocean (Rachold et al. 2004; McGuire et al. 2009; Vonk et al. 2012). There, it either is buried in the shelf sediments, exported to the ocean, or mineralized by bacteria and then emitted to the atmosphere as a greenhouse gas, thus being able to contribute to further global warming (Rachold et al. 2005; McGuire et al. 2009; Couture 2010; Vonk et al. 2012). Therefore, detailed investigations of coastal retreat are necessary for reasonable estimates of greenhouse gas emissions, which in turn serve as a basis for predictions of future climate change (McGuire et al. 1995; Zhang & Chen 2005). The international Arctic Coastal Dynamics project compiles data from numerous monitoring sites across all arctic coasts with the goal of estimating sediment fluxes on a circum-Arctic scale (Brown & Solomon 1999; Rachold et al. 2004; Rachold et al. 2005; Lantuit et al. 2011). Total organic carbon supply resulting from coastal erosion to the Arctic Ocean is estimated at 6-7 * 10^6 metric tons C/a (Rachold et al. 2004), therefore amounting to approximately 10 to 15% of the overall estimated annual organic carbon input into the Arctic Ocean (McGuire et al. 2009; Ping et al. 2011). In some areas with very high coastal erosion rates, like for example along the Laptev Sea, the amount of sediments supplied by coastal erosion to the sea can highly overtop the amount contributed by rivers. Even along stretches of the Beaufort Sea coast, sediments delivered by coastal erosion can locally exceed the rate of fluvial sediment supply, although most of the sediment is of fluvial origin (Reimnitz et al. 1988; Brown & Solomon 1999; Rachold et al. 2000).

For the reasons given above, it is of major importance to investigate coastal change in the Arctic, as these investigations provide the basis for assessments of coastal response to changing external conditions. The observation of how Arctic coasts respond to a changing climate, which feedbacks occur, and which factors seem to be of greater or lesser importance for coastal change, gives us the opportunity to draw conclusions on what we can expect to happen along these coasts in the future (Hinzman et al. 2005).

The focus of this work is the western coast of the Yukon Territory, Canada (Appendix I). Because this area has some of the highest ground ice contents (Lantuit et al. 2011) and is exposed to the north and partially to the north-northwest, which is the direction from which the most effective storms originate (Reimnitz & Maurer 1979; Hudak & Young 2002), coastal erosion is likely to increase in this region in the future (Forbes & Taylor 1994; Manson & Solomon 2007; Lantuit & Pollard 2008). Therefore, a detailed assessment of coastal change in the western Yukon Territory is of particular interest.

Despite the remoteness of this region, some data exists to enable calculations of coastal retreat rates for the USA-Canada border beginning as early as 1912 (Table 1). Over the years, a broad range of studies focusing on coastal processes has been carried out along the Yukon coast, as well as the neighboring Alaskan Beaufort coast which, due to its similar geomorphology and wave exposure, is comparable to the Yukon coast (Forbes 1997). Results from studies monitoring coastal change along both coasts show a wide range of erosion rates (Table 1). The assessment of coastal change by means of aerial photography and field site visits only provides a snapshot of the coast, so it is thus highly dependent on the climatic conditions at, or just prior to, the investigation (Solomon & Gareau 2003). Analyses of aerial photographs of Herschel Island indicate that erosion decelerated from 0.61 m/a between 1952 and 1970 to 0.45 m/a between 1970 and 2000 (Lantuit & Pollard 2008). These results are consistent with findings from the Mackenzie Delta region which also show a deceleration of erosion from 1.02 m/a between 1972 and 1985, to 0.87 m/a between 1985 and 2000 (Solomon 2005). In contrast, since the early 1980's doubling of erosion rates to 25 m/a has been measured at an Alaskan coastal site (Mars & Houseknecht 2007; Jones et al. 2008; Jones et al. 2009). A doubling of erosion rates along the Alaskan Beaufort Sea coast was also measured by Ping et al. (2011), who determined present rates to be 1.2 m/a using aerial photography and satellite imagery analysis. For the western Yukon coast, only a limited amount of data from field surveys and aerial photography analyses are available. They show that, at the eastern fringe of the study area some 35 km to the east of the USA-Canada border, there was a general deceleration of coastal erosion between the 1950's (~ 3 m/a) and the late 1990's (< 1 m/a) (Harper et al. 1985; Forbes et al. 1995; Solomon 1998), and that at the USA-Canada border, there was an acceleration of coastal change from < 1 m/a between 1912 and the mid 1980's to about 2 m/a between the 1980's and 2000 (McDonald & Lewis 1973; Forbes & Frobel 1985; Ping et al. 2011). However, no recent and consistent long-term regional assessment of coastal change currently exists for the Canadian side of the border (Table 1).

Table 1: Literature review of erosion rates (ER) for the investigation area (in bold). Some additional erosion rates for nearby regions are included for reference. Erosion rates are listed by region, going from east to west. For exact location of the sites, see Appendix I.

Citation	Data base	Region	Time frame	ER [m/a]
Solomon 2005	Aerial photography	Tuktoyaktuk Peninsula to Mackenzie Delta	1972-1985	-1.02
			1985-2000	-0.87
McDonald & Lewis 1973	Aerial photography	Kay Point, eastern Yukon	1952-1970	-2.3
Forbes & Frobel 1985	Geodetic survey	Kay Point, eastern Yukon	1976-1984	-1.3
Forbes et al. 1995	Geodetic survey	Kay Point, eastern Yukon	1984-1992	-3.0
Lantuit & Pollard 2008	Satellite imagery, aerial photography	Herschel Island, western side	1952-1970	-0.61
			1970-2000	-0.45
Forbes et al. 1995	Geodetic survey	**Komakuk, western Yukon**	1986-1991	**-0.76**
			1991-1992	**-0.60**
Solomon 1998	Aerial photography, geodetic survey	**Komakuk, western Yukon**	1951-1958	**~ -3.0**
			1960-1971	**~ -2.0**
			1975-1997	**< -1.0**
Harper et al. 1985	Video, aerial photography	**Komakuk to Clarence Lagoon**	1950's-1984	**-1.06**
Covill 1997	Aerial photography	**Clarence Lagoon, western Yukon**	1976-1992	**-0.08 - -0.49**
			1992-1996	**-0.29 - -1.64**
Harper et al. 1985	Video, aerial photography	**Clarence Lagoon to USA-CAN border**	1950's-1984	**-1.28**
McDonald & Lewis 1973	Geodetic survey	**USA-CAN border**	1912-1972	**-0.72**
Forbes & Frobel 1985	Geodetic survey	**USA-CAN border**	1972-1984	**-0.83**
Ping et al. 2011	Satellite imagery, aerial photography	**USA-CAN border**	1950-1980	**-0.74**
			1980-2000	**-3.88**

Brown et al. 2003	Satellite imagery, aerial photography	Barrow, Alaska	1948-1979	-0.59
			1979-2000	-0.86
Jones et al. 2009	Aerial photography	Barrow, Alaska	1955-1979	-6.8
			1979-2002	-8.7
			2002-2007	-13.6
Ping et al. 2011	Satellite imagery, aerial photography	Alaska Beaufort coast	1950-1980	-0.6
			1980-2000	-1.2
Gibbs et al. 2011	Aerial photography	Demarcation Point – Brownlow Point	1947-2007	-0.6 ± 0.4
		Alaska Beaufort coast		-2.0
Lantuit et al. 2011	ACD database	Canadian Beaufort coast		-1.12
		Entire Arctic coast		-0.5

So far, no single research approach has been able to adequately explain the especially high erosion rates which are occurring in the Arctic. Although there is broad scientific agreement that the existence of ice-rich fine grained coastal sediments, the stormy nature of the Arctic Ocean, and the presence of ice in the water column as well as in the nearshore zone all contribute to observed shoreline dynamics, opinions about the significance of each factor are deeply divided.

Some of the research has focused on the correlation between coastal erosion and oceanographic forcing, such as sea level rise, waves and storms (Reimnitz & Maurer 1979; Solomon et al. 1994; Héquette et al. 1995; Manson & Solomon 2007); these studies suggest that storms are very effective erosive agents and that predicted increase in open water season and sea level will foster their erosive action. Valuable information about regional wave climatology is provided by the extreme wave hindcast study conducted by Eid & Cardone (1992) and the study on storm patterns conducted by Atkinson (2005). Physics-based modeling approaches on the effect of storm surges have been conducted for example by Kobayashi (1985), Kobayashi et al. (1999), Hoque & Pollard (2008, 2009) and Ravens et al. (2012).

Further studies concentrate on the contribution of ground ice and permafrost to high erosion rates (Harper et al. 1985; Kobayashi 1985; Aré 1988; Harper 1990; Héquette & Barnes 1990; Dallimore et al. 1996; Kobayashi et al. 1999; Lantuit et al. 2008). A number of researchers have concluded that the characteristic coastal composition, consisting of fine grained, ice-rich and thus mostly unconsolidated sediments, contributes to or even governs rapid coastal change in the Arctic (Reimnitz et al. 1985; Reimnitz et al. 1988; Jorgenson & Brown 2005; Aré et al. 2008). In modeling of coastal response to future climate change conducted by Couture (2010), the combination of ground ice content and effective cliff height was shown to be important for future coastal erosion, with a predicted acceleration of low bluff erosion (Couture 2010). Findings from the Arctic Coastal Dynamics project, however, reveal only a minor correlation between backshore elevations and coastal retreat (Lantuit et al. 2011).

Héquette & Barnes (1990) correlated erosion rates with both, coastal geology (sediment texture, ground-ice content, cliff height, shoreface gradient) and oceanographic forcing (wave energy) and found no statistical relationship which would adequately explain the variability and amount of erosion. Thus they

presumed that another factor has to play a major role in arctic coastal retreat. Under the assumption, that the shoreface profile always strives for a state of equilibrium (Bruun 1954), they concluded that modifications of the nearshore profile by ice gouging of the seabed may be highly effective in forcing coastal retreat by lowering the nearshore profile. Another process influencing the local bathymetry is thaw subsidence induced by permafrost melt in the shallow water zone. It was investigated by Reimnitz et al. (1985, 1988) and Reimnitz & Aré (1998) who studied the relative contribution of thaw settlement in the nearshore zone to the deepening of the nearshore profile. According to their findings, only about 14% of nearshore profile deepening can be attributed to thaw settlement and in water depths exceeding 1.5 m no profile deepening could be attributed to this particular process (Reimnitz & Aré 1998). Further studies conducted by Hume et al. (1972) and Kobayashi et al. (1999) also prove that the recovery of the eroded beach profile plays an important role in the erosion pattern of the coast. In addition, Kobayashi et al. (1999) modeled the retreat of a frozen cliff fronted by a beach during a storm and subsequently used this model to evaluate the significance of several factors for shoreline retreat. According to their findings, storm surge elevation and duration, seawater temperature and salinity, cliff height and sediment characteristics all play a significant role in the processes regulating coastal retreat.
The observed high spatial and temporal variability in coastal change (Dallimore et al. 1996; Forbes 1997; Brown et al. 2003; Manson et al. 2005; Solomon 2005) prove the fact that, especially in such a cold climate environment a wide range of factors contributes to coastal dynamics. It seems like their significance cannot be determined in an unambiguous way, but has to be defined in consideration of the specific site and conditions.

Aims and Objectives

As outlined above, despite the high likelihood of an acceleration of coastal retreat along the western Yukon coast due to changing climatic conditions, no regional investigations have recently been conducted to allow a detailed and consistent quantification of coastal dynamics in this area. Therefore, the primary goal was to calculate long term coastal change rates on the basis of remote sensing data for the entire investigation area, as well as to update and analyse recent and previous field survey data at two GSC monitoring sites located at the margins of the study area. A subsequent detailed evaluation of the research results aims to examine the spatial and temporal variability of the coastal dynamics, and whether geomorphological parameters like beach width or cliff slope can explain this variability. The findings attempt to contribute to a better understanding of factors which govern coastal behavior in a changing high latitude environment. By the establishment of a detailed coastal change rate data base, this work also aims to provide a reliable foundation for future regional coastal research like for example detailed assessments of sediment and carbon fluxes into the Beaufort Sea.

Study Area

In order to investigate the variability of coastal change rates, a section of coast extending 35 km along the Arctic coast of the western Yukon Territory was selected as a study area (Figure 1). Its western boundary is marked by the Canada-USA border (69°38'46"N, 141°00'00" W), whereas the eastern boundary is given by the Komakuk DEW line station (69°35'51"N, 140°10'45"W). The study area lies within the boundaries of the Ivvavik National Park and outside the influence of the Mackenzie River, which enters the Beaufort Sea well east of Komakuk. As the studies were focused on the boundary areas of the study area (subsequently called Border site and Komakuk site), descriptions for both, the whole study area with focus to the Border and Komakuk site are provided.

Figure 1: The study area is located in the western Yukon Territory and is limited by the Canada-USA border to the west and the Komakuk DEW line station to the east.

Geology and Geomorphology

The study site is situated within the Yukon Coastal Plain, a 10 to 40 km wide smooth lowland which is flat to gently sloping towards the bordering Beaufort Sea in the north (Forbes 1997). To the south it is fringed by the British Mountains which have an average height of 460 to 600 m and in general do not exceed 780 m (Rampton 1982). Stream valleys and small thermokarst basins are incised into the hilly tundra terrain as deep as 15 m below the general level of the plain (Rampton 1982). Offshore, the approximately 60 km wide continental shelf slopes gently from the coastal lowlands to the 80 m deep shelf break up (Hill et al. 1991). The coastal plain constitutes the landward extension of the Beaufort shelf and is covered with Pleistocene and Holocene unconsolidated deposits, primarily gravels, sands and silts (Norris 1975; Rampton 1982). These are ice-bonded, since the whole coastal plain and part of the sea bed are underlain by several hundreds of metres thick permafrost. Permafrost is, by definition, soil which remains frozen for at least two consecutive years (Brown & Kupsch 1974). The study area is underlain by continuous permafrost, meaning that permafrost is present everywhere, except beneath large lakes and rivers (Brown & Kupsch 1974; Rampton 1982). As numerous rivers and streams flow through the Yukon Coastal Plain, like the Backhouse River just east of Clarence Lagoon, or Fish Creek near Komakuk, some of the sediments are of fluvial origin, partly covered by organic veneer. However, most of the study site is composed of marine and estuarine deposits (Norris 1975). During the Wisconsin Glaciation, the maximum glaciation extension of the Laurentide Icesheet in this region went as far west as Firth River, thus not affecting the study area (Rampton 1982). As a result, the diverse mixture of marine, deltaic, fluvial, lacustrine and terrestrial sediments which was deposited on the Yukon Coastal Plain prior to the glaciation can still be seen in exposed bluffs along stream channels and the coast (Rampton 1982).

Periglacial processes which are geomorphological processes and deposit characteristics of frost-affected margins of existing and former glaciers, dominate the morphology of the study area, as the sediments are subject to extensive frost-action (Brown & Kupsch 1974; French 2007).
The permafrost stratum is covered by the active layer, the top layer of ground that thaws each summer and refreezes each fall (Brown & Kupsch 1974). In 2012, at the Border site active layer measurements indicated depths between 33 cm and 112 cm. As the depth of the active layer is dependent on many different factors, like air temperature or snow cover, it can vary significantly between years and sites, but with consistent long-term monitoring, it can be taken as an indicator for climate change (Couture & Pollard 2007; French 2007). In the study area, permafrost contains vast amounts of ground ice which is mostly present as pore ice, massive ice, segregated ice and ice wedges. This suggests, that the physical properties of frozen ground are more closely related to these of ice or even rock, than to those of soil (Couture & Pollard 2007; Aré et al. 2008). Ice wedges are very characteristic features of periglacial processes, as they lead to the formation of polygonal patterned ground. The foundation for their genesis is built during winters when the ground contracts due to low temperatures and subsequently cracks. During spring, surface meltwater intrudes into these cracks and freezes. This process repeats every year along the same thermal-contraction cracks, evoking the gradual build-up of ice wedges. During the summer months the top of the ice wedge melts and troughs develop, leading to polygonal pattern, which can be seen from aerial perspective (Figure 2) (French 2007).
A further periglacial process which shapes the morphology of the Yukon Coastal Plain is thermokarst development, a physic-geological process which leads to the formation of subsided and collapsed relief forms due to local deep thawing of permafrost layers and underground ice (Aré 1988, after Katasonov & Solov'yev 1969; Harry 1988). The occurrence of numerous thermokarst depressions of various sizes, leading to the genesis of lakes and ponds, is a result of these processes (Harris et al. 1988).

Arctic coastal processes

In the Arctic, coastal dynamics are additionally influenced by cryogenic factors, such as permafrost in the coastal cliff or sea ice in the water column. The following sections give an overview over coastal processes which are unique to cold climate regions.

Thermal abrasion

Within the study area cliffs are mainly composed of frozen silty sediments with high ice contents. Exposed at the cliff face, these sediments thaw and turn into fluid mud, thus on average losing up to 60% of their original volume (Aré et al. 2008). When water reaches the cliff toe, these sediments can be easily redistributed. Because a large part of the permafrost volume is diminished by thawing, the effects of coastal erosion can be greater on ice-rich shorelines (Aré et al. 2008). The majority of cliff erosion takes place during storms and is driven by thermal abrasion, the combined effect of the mechanical and thermal influence of the salt water. The turbulence of storm waves causes net onshore transfer of heat inside the surf zone, leading to rapid melting of the lower cliff face and beach accelerating the thawing of ice-rich sediments (Aré 1988; Kobayashi et al. 1999). This can lead to the genesis of a thermo-erosional niche (Hoque & Pollard 2009) and when polygonal patterns erode, block failures may occur (Figure 2) (Reimnitz & Maurer 1979; Reimnitz et al. 1985; Forbes & Taylor 1994; Jones et al. 2009). This process occurs partially due to the presence of ice wedges in the cliff, which dissect the soil layer perpendicular and parallel to the shoreline and create lines of weakness. When the thermo-erosional niche extends far enough under the cliff, the force of gravity exceeds the cohesive force of the ice wedge leading to block failure and temporary protection of the newly created cliff face (McDonald & Lewis 1973; Aré 1988; Hoque & Pollard 2009). Fine grained sediments (silt and clay) are transported offshore, while coarser fractions (sand and gravel) are transported along shore and build protective beaches and spits (McDonald & Lewis 1973). The critical depth of the thermo-erosional niche is dependent on the cliff height, soil composition and ice wedge proximity to the cliff face. High cliffs, for example, can fail without the presence of a thermo-erosional niche, if the ice wedge is close enough to the cliff face, or if the cliff reveals a very high concentration of ice wedges (Hoque & Pollard 2009).

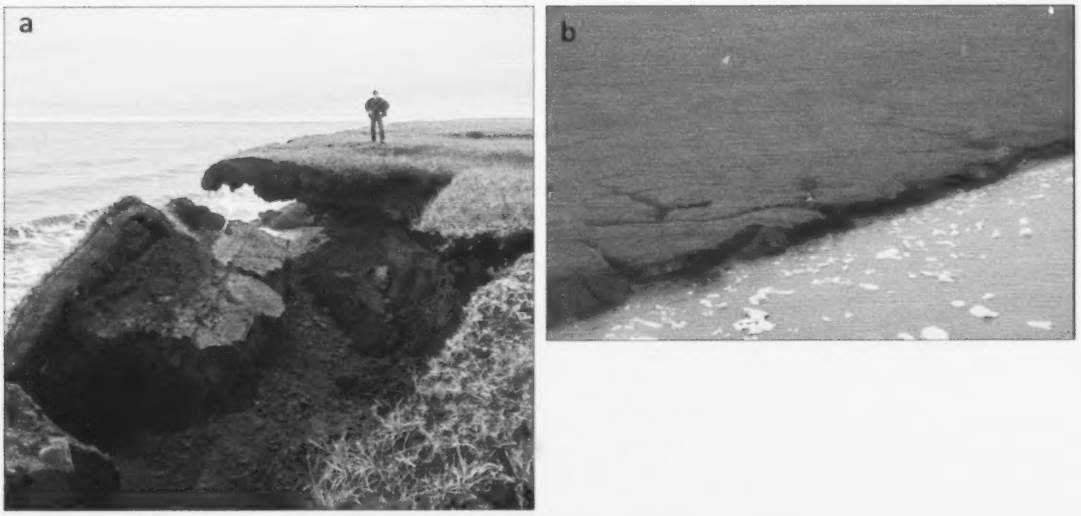

Figure 2: a) Example of a collapsed tundra polygon and an approximately 2 m deep erosional niche; b) Coastline in between Komakuk and Clarence Lagoon, dominated by block failures. Photos: A. Konopczak, 2012.

Thermal denudation

Thermal denudation is a process leading to the erosion of material under the influence of heat stored in air or water or in the form of solar radiation. Material which is exposed at the cliff face experiences thermal denudation during summer, resulting in the thawing and downslope transport of sediments. In areas, where thermal and mechanical abrasion by waves is slower, or the thermal denudation of the cliff proceeds comparatively faster, the thawed material can accumulate on the foot of the slope, creating an insulating layer and smoothing the cliff slope (Aré 1988). These cliffs are fronted by active low-angle irregular slopes of partly thawed tundra (Figure 3).

Thermal denudation can also affect subsea permafrost. When subsea permafrost thaws due to the influence of the comparatively warmer water, thaw subsidence of the sea floor can occur. This leads to a local increase of water depth and steepening of the shoreface slope, such that higher waves can approach closer to the shoreline, with larger erosive power (Aré et al. 2008); however only a minor percentage of coastal erosion can be attributed to this process (Reimnitz & Aré 1988).

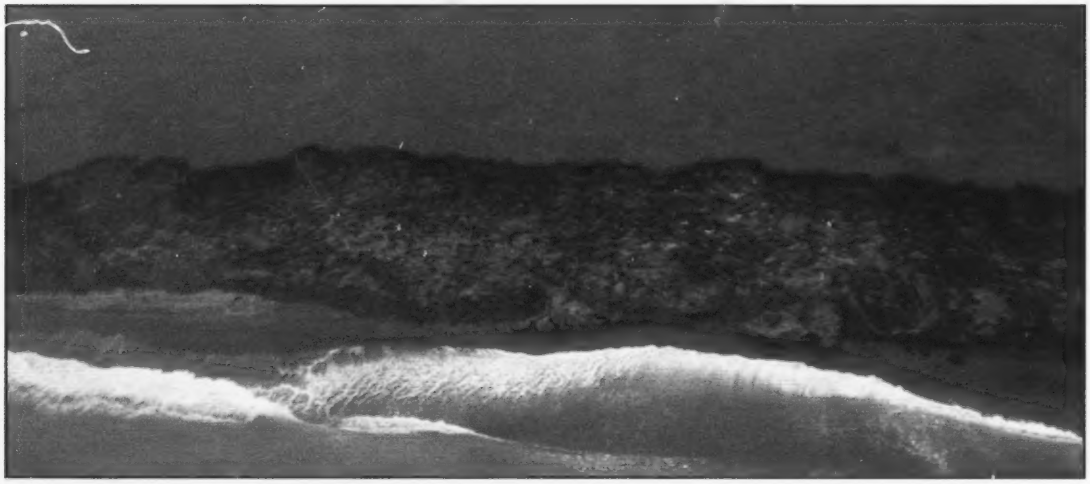

Figure 3: Coastal stretch to the west of Clarence Lagoon shows result of faster thermal denudation of the cliff face than thermo-mechanical abrasion of the cliff slope. Photo: A. Konopczak, 2012.

Sea ice processes

Sea ice processes play a major role for the coastal sediment budget as they are capable to erode, transport and accumulate sediments throughout the nearshore zone (Héquette & Barnes 1990; Reimnitz et al. 1990; Ogorodov 2003). Previous research shows that the highest storm winds, waves and surges occur in October, at the end of the open water season (Hudak & Young 2000; Atkinson 2005; Manson & Solomon 2007). During ice freeze-up and break-up, storms gain additional erosive power by sea ice in the water column. Carried by storm waves and pushed against the shore, this ice can cause considerable cliff and beach modification through abrasion (Reimnitz et al. 1985). But sea ice can lead to net sediment supply, too, for example by ice ride-up when ice sheets slide over beaches and barriers and supply sediments from the shallow shoreface (Reimnitz et al. 1990). Ice pile-ups, generated by onshore push and subsequent crumble and pile-up of ice sheets to heights of as much as 20 m can deposit sediments on top of cliffs, or create ice ramps which facilitate wave run up (Reimnitz et al. 1990; Aré et al. 2008). Forbes & Frobel (1985) and Forbes & Taylor (1994) reported on beach sediment occurrences on cliff tops at and near.

A process which can considerably alter the nearshore seabed as well as the shoreface is ice wallowing. Ice wallowing occurs, where sea ice freezes to the seabed and is moved by waves, thus locally altering the seabed relief (Hill et al. 1994). Temporary nearshore bathymetry changes can occur through ice gouging, when ice floes are dragged through nearshore sediments creating deep and steep flanked trenches (Héquette & Barnes 1990).

The described sea ice processes do not result in permanent changes, but are capable of modifying local onshore and nearshore relief for up to a few years, thus leading to temporary changes in the shoreface profile (Hill et al. 1994). According to Bruun (1954), the shoreface profile always strives for a state of equilibrium thus nearshore deepening is compensated with onshore sediment supply meaning that erosion of the beach and cliff face can occur. Consequently ice processes are capable of annually influencing the local sediment budget and coastal dynamics.

Vegetation

The Yukon Coastal Plain lies well beyond the limits of tree growth and is primarily covered by herbaceous vegetation forming tussock tundra (Welsh & Rigby 1971; TAGA 2013). Mosses, grasses and sedges are also present at the Komakuk site, whereas the vegetation cover at the Border site is dominated by short grasses with very shallow roots, penetrating less than 15 cm into the active layer. The vegetation cover bonds the upper part of the soil, leading to overhanging vegetation mats at some eroding cliff sites.

Climate

The western Yukon Coastal Plain is dominated by a harsh and cold Arctic climate (Rampton 1982). Komakuk climate data for the years 1971 to 2000 show a mean annual temperature of -11°C, with lowest mean temperature in February (-25.3°C) and highest mean temperature in July (7.8°C). Extremes range from a low of -51.8°C to a high of 30.2°C (National Climate Data and Information Archive 2013a). A comparison of the temperature records from the months June to August of the time period from 2000 to 2002 to records from 2010 to 2012 reveals an apparent increase of mean temperatures amounting to 2.3 °C (National Climate Data and Information Archive 2013b).

Rainfall data from 1971 to 2000 for Komakuk show a mean value of 83.5 mm/a, whereas mean annual snowfall is 77.7 cm. Approximately half of the precipitation falls as snow, covering the study site on average 255 days per year (National Climate Data and Information Archive 2013a).

According to the Komakuk climate statistics, there are two main directions of maximum wind speeds. During the ice free period maximum winds from the east dominate, whereas maximum winds blowing from the west are more common during the winter months and are generally slower, than during the winter (National Climate Data and Information Archive 2013a).

Sea ice

Sea ice usually covers the shore from the first week of October till the last week of June, thus leaving the shore ice free for approximately 104 days (Couture 2010).

Only then coastal erosion can be caused by storms as in the remaining time, sea ice protects the shoreline from wave impact (Forbes & Taylor 1994; Atkinson 2005). During the ice free season, the extent of open-water fetch varies annually, depending on atmospheric forcing, oceanic circulation and local conditions (Mysak & Manak 1988; Hill et al. 1994; Johannessen et al. 2004) such that seasonal wave energy can be highly variable. Ice-free fetch can be as high as 200 km in years with comparatively high sea and air temperatures resulting in small ice cover but can be as low as 20 to 50 km during years with heavy ice cover conditions (Forbes 1997). Commonly, the longest fetch distances occur in late August (Hill et al. 1994), but in high ice years sea ice remains against the coast during the whole summer (Forbes 1997). Even during mild summers, pack ice sometimes approaches the coast, as was observed during the field survey in early August 2012.

Water levels

As the Yukon Coastal Plain lies in the microtidal zone, astrological tides usually do not exceed 0.5 m (Harper 1990), and 80% of water level variability can be attributed to winds and air pressure (Forbes 1997).

Analyses of water level measurements from Tuktoyaktuk, a hamlet located approximately 270 km east of Komakuk, indicate that subsidence and eustatic changes evoked an increase of relative sea level rise of 3.5 + 1.1 mm/a since 1961 (Manson & Solomon 2007). Assuming that relative sea level rise is going to accelerate due to the addition of meltwater from glaciers on land and steric effects, a further relative sea level rise of 0.76 m by 2100 is expected (Manson & Solomon 2007).

Storms

Storms, defined as winds blowing at a speed of at least 10 m/s for at least 6 hours (Solomon et al. 1994; Atkinson 2005), are most effective when gale winds are coming from the west to north-west, as this creates positive storm surges (Hill et al. 1994; Solomon et al. 1994). Onshore winds are predominant

during the open water season, so that the majority of storms affect the coastline, with significant wave heights reaching 4 m or even more and peak periods of 10 seconds (Solomon et al. 1994, after Pinchin et al. 1985). These high water events are major drivers of coastal modification processes, as by overtopping beaches and barriers, they are enabling direct wave attack at the cliff base (Reimnitz & Maurer 1979). Statistical analyses of storms during the open water seasons of the years 1950 to 2000 yielded that on average 18.5 storms occur in the Beaufort Sea each year, with mean storm core speeds (mean of the speed values in the upper 50th percentile of all the winds of one event) and mean storm maximum speeds rising throughout the season to 10.8 m/s and 12.8 m/s, respectively (Atkinson 2005). Mean core winds duration is highest in June (22 h) and October (24 h) (Atkinson 2005).

Study site descriptions

Border site

The Border site lies at the western end of the study area. The mean cliff height at the Border site is 5.6 m. The cliff faces the Beaufort Sea to the north, is moderately sloping and does not have thermo-erosional niches or cliff overhangs (Figure 4). When surveyed (first half of August 2012), no massive ice or ice wedges were observed, yet gullies in the cliff wall indicated a vast amount of ice in the soil and ice wedges form distinct polygonal patterns in the tundra. The average cliff slope is 34° and it consists of very fine sediments, with an estimated dominant grain size in the range of silt to silty clay with pebbles and small cobbles. Vegetation mats of various sizes are detached from the cliff top and partly cover the cliff face. Fronting the cliff is a relatively narrow beach (6 m) consisting of pebbly sand with patches of coarse gravel. The beach has a mean slope of 7.2°, which allows wave run-up to reach the cliff toe even during non-stormy conditions. Based on the site morphology, the dominant coastal erosion processes seem to be runoff, gully development and gravity failures.

To the west of the study site lies the Alaskan Coastal Plain. This region, extending west to Demarcation Bay, is similar to the western Yukon Coastal Plain in terms of geology and geomorphology. Further west, the coastal geomorphology changes abruptly to barrier islands which are backed by shallow lagoons (Lewellen 1973). Demarcation Bay is an approximately 6 km wide lagoon which is fed by the Turner River as well as Putugook and Kagiluak creeks. This lagoon is located approximately 9 km west of the Border site and may constitute the primary sink for nearby sediment.

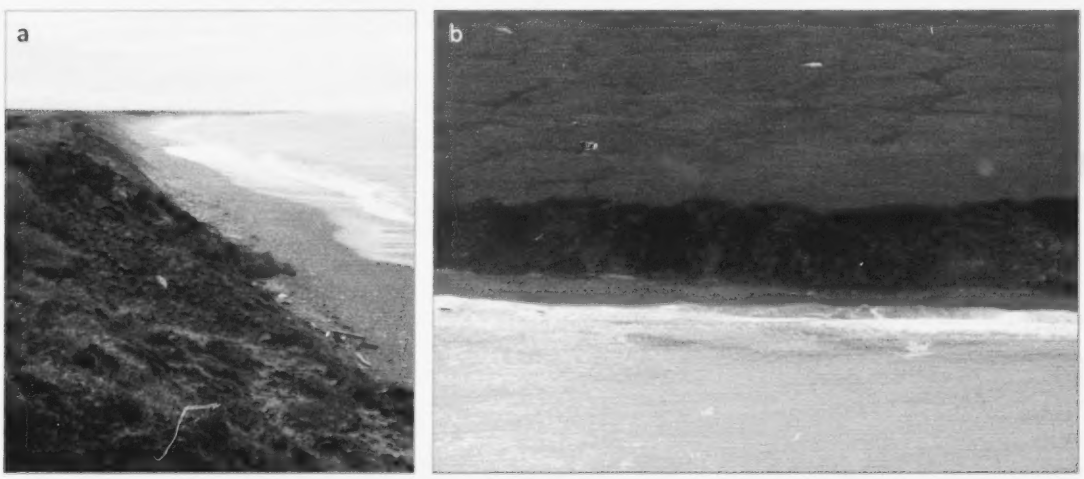

Figure 4: a) The cliff morphology at the Border site shows slumps rather than overhangs and the cliff face is partly covered with small detached vegetation mats. b) Approximately 2 km further east the cliff face is steeper with overhanging vegetation matts and is fronted by a narrower beach. Photos: A. Konopczak, 2012.

Komakuk Distant Early Warning Line Station

A large part of the Komakuk study area is influenced by a radar station, which was constructed in between 1952 and 1957 as part of the Distant Early Warning (DEW) line (Moore 2011). The DEW line stations were built in order to detect Soviet missile attacks and thus protect North America during the Cold War, but technological advance led to the abandonment and automation of stations (Lackenbauer et al. 2005). The Komakuk station was automated in 1993 and staff were relocated (PC 2009). During the construction and operation of the station, major damage to the vegetation cover occurred, since heavy equipment disturbed the tundra, triggering permafrost melt and terrain degradation. Moreover, at least four major landfills consisting of garbage, fuel drums, PCB containers and other hazardous materials were buried in the tundra, thus causing environmental pollution (PC 2009). Even after the clean-up of the site, where most of the garbage was excavated, buried drums can still be seen in the cliff face at Komakuk.
The most essential alteration of the local environment which greatly modifies the coastal zone is the presence of an airstrip and adjacent roads, which were constructed of one to two metres of gravel compacted on top of the ice-rich tundra (Solomon 1998).

Komakuk site description

The Komakuk site lies at the eastern end of the study area. Tundra polygons as well as thermo-erosional gullies and ponds characterize the backshore morphology of the Komakuk site which occupies a topographic high, with gentle slopes east towards the Malcom River and approximately 1 to 2 km to the west. The site is exposed to the Beaufort Sea with a north-north west aspect. Coastal recession leads to erosion of the airstrip and an adjacent road to the east. The airstrip is not eroding as fast as the local polygonal tundra landscape, and forms a small promontory at the highest part of the cliff.
The coastline west of the airstrip differs significantly from the coastline to the east. The western section consists of up to 4 m high vertical to overhanging cliffs, with exposures of massive ice where tundra polygon wedges intersect in the cliff face. The volumetric ground ice content of the local soil amounts to 61% (Couture 2008). The cliff face can be roughly subdivided into two stratigraphic units, the comparatively ice-poor greyish silt to sand unit, reaching from the cliff toe up to approximately 2 m above ground and the overlying 2 m thick ice-rich peat unit (Fritz et al. 2012). The transition from one unit to the other is visible by a niche in the cliff, presumably resulting from the faster erosion of the lower unit (Figure 6 a) 1). The cliffs are topped by overhanging vegetation mats and groundwater percolation as well as run-off is observed along the cliff face. At the western limit of the Komakuk site, a drainage channel filled with driftwood is fronted by an approximately 60 cm high berm. The beach fronting the western section of the study site is 9.5 to 12 m wide with an average slope of 7° and consists of coarse pebbly sand. Based on the site morphology, the dominant coastal erosion processes seem to be gully development, basal wave cut as well as gravity and block failures.
The cliff morphology changes abruptly at the airstrip (Figure 6 b). The 6.5 m high cliff face is partially protected by gravel eroded from the upper 1-2 m thick airstrip. This gravel appears to be the major component of the 20 m wide beach fronting the cliff. With 5° and 36° respectively, the beach and cliff slopes are more gentle than those to the west. Longshore drift appears to transport the gravel eastwards and contributes to the build-up of a broad (25 m wide), very gently sloping (2°) beach immediately adjacent to the eroding airstrip.
Further east of the airstrip, the shoreline morphology again changes. Instead of a high, steep cliff with sharply defined tundra polygons delineated by ice wedges, there is a low, gently sloping (8°-13°), eroding vegetated tundra slope. Just east of the airstrip a road has eroded and created an artificial low cliff. Driftwood is found at the beach and on top of the cliff, indicating this is an area of both deposition and storm wave erosion.

Figure 5: a: Overview of the Komakuk study site with indicated sections 1 to 3; a) 1: in section 1 the cliff face reveals a thermo-erosional niche, which is formed due to a lower ice content in the lower stratigraphic unit, the eroding tundra polygons contain vast amounts of ground ice; a) 2: the eroding gravel airstrip builds section 2; a) 3: section 3 is characterized by single degraded low tundra polygons. b: Photo shows abrupt change from section 1 to section 2. GPS rod height is 2 metres. Photos: G. Manson, 2012.

The coast between the Komakuk and Border sites

Based on morphology and composition, the coast between the Komakuk and Border sites can be roughly divided into two sections, separated by Clarence Lagoon (Figure 1), a 3 km wide lagoon located 6.5 km east of the international border.

The eroding cliffs between Komakuk and Clarence Lagoon are mainly composed of fine grained, ice-rich sediments, which are to a great extent covered by a peat layer in the upper part of the cliff face. The shoreline just west of Komakuk consists of 3 to 5 m high cliffs with tundra polygons separated by gullies filled with sand and, depending on their size, occasionally driftwood (Figure 6 a). The low cliffs are fronted by an approximately 7 to 10 m wide beach. Adjacent to this area to the west, the local cliff exposure changes from north-west to north and a cohesive overhanging cliff face with deep thermo-erosional niches forms the shoreline (Figure 6 b). During field surveys in August 2012 no beach was distinguishable and the swash reached the cliff toe. This coastal stretch is the only region of the study area which has block failures (Figure 6 b). West of the block failure area the coastline is alternately comprised of notched, slumping or very steep and homogeneous cliffs which form a straight shoreline (Figure 7 c). All cliff forms are fronted by narrow beaches. Many channels, creeks and small rivers, such as the Backhouse River, enter the Beaufort Sea between Komakuk and Clarence Lagoon. At tidal channels in barrier beaches and at river deltas, the beaches locally widen, the shoreline profile is more gently sloping and cliffs are often absent (Figure 6 d). To the east and west of the Backhouse River thermal denudation processes predominate, leading to cliff faces which are fronted by a smooth broad slope (chapter thermal denudation). This area has the highest cliffs between Komakuk and Clarence Lagoon (Figure 6 e), with heights up to 10 m. Just east of the lagoon is an area which is comprised of vast amounts of peat. The section ends at Clarence Lagoon, which is fed by numerous streams.

In contrast to the coastal stretch between Komakuk and Clarence Lagoon, the shorter section between Clarence Lagoon and the Border site is more homogenous, does not seem to experience thermo-erosional notching, and appears to have no peat. The coastal geomorphology is comparable to that of the Border site with comparatively smoother, slumping cliffs consisting of fine grained ice-bonded sediments (Figure 6 f). Just west of the lagoon, two 600 to 1000 m long coastal stretches occur, where the process of thermal denudation determines the shape of the cliff face. Moving west from Clarence Lagoon, cliff heights rise quickly and reach a height of up to 11 m approximately half way between the Lagoon and the Border, and subsequently diminish in height to less than 6 m at the Border site. The cliffs are faced by generally narrow beaches which seem to widen in front of higher cliff faces. Many erosional gullies dissect the cliff face, but no rivers or creeks enter the Beaufort Sea in this section except for two small channels close to the Border site.

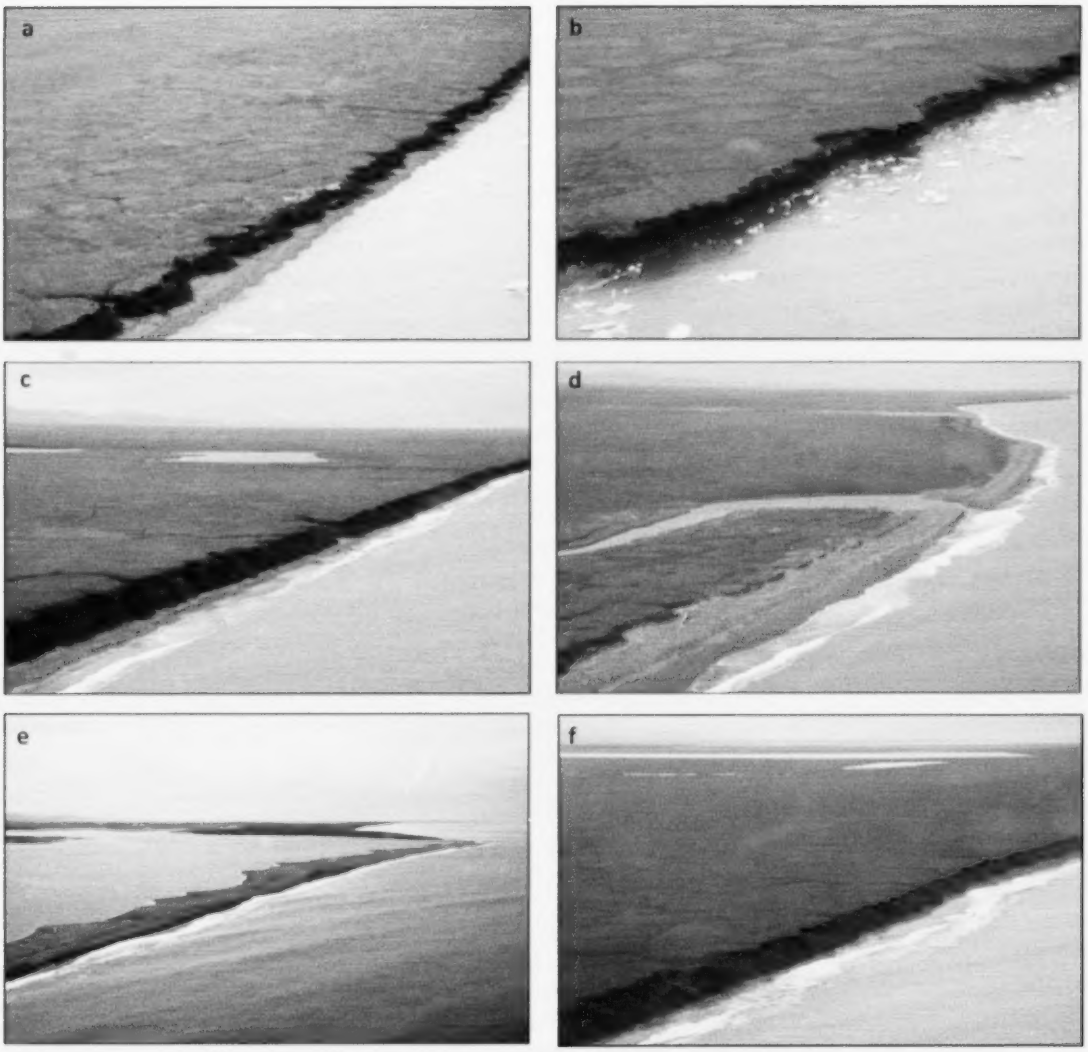

Figure 6: Coastal morphology between Komakuk and the Border site, going from east to west; a) low deeply dissected tundra polygons with sand accumulations in between, b) area with deep thermo-erosional niches, c) steep, high cliffs forming a straight shoreline, d) low relief shoreline in the area of an entering stream channel, e) spit forming Clarence Lagoon, f) high but comparatively smoother cliffs comprising the shoreline near the Border site. Photos: D. Forbes & A. Konopczak, 2012.

Data and Methods

The sources of data for shoreline change calculation are remote sensing data, consisting of aerial photographs and satellite imagery, and field survey measurements collected using a theodolite infra-red station, or Real Time Kinematic-Global Positioning System (RTK-GPS) (Figure 7). While remote sensing was used for conducting shoreline change analyses of both study sites and the area in between in order to gain insight into on-going processes and long term trends, the field survey data allowed a more local and accurate analysis of shoreline change over the last two decades. The following sections provide information about data acquisition, quality, and processing.

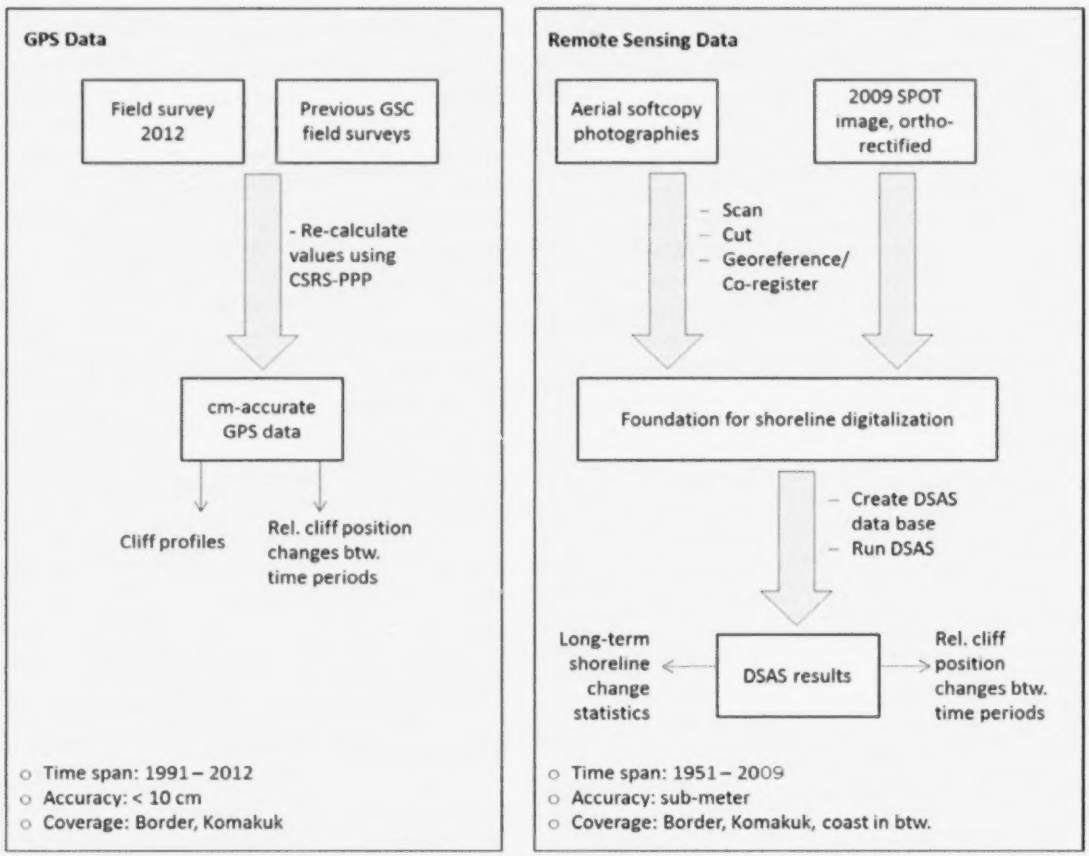

Figure 7: Data preparation and processing

Field survey data

The study area was investigated in a field survey in the first half of August 2012 (04.-18. Aug). During this time, RTK-GPS measurements at both study sites were made in order to investigate local shoreline conditions with centimetre accuracy. This high accuracy was chosen in order to minimize position uncertainties, resulting from equipment restrictions. Together with data from previous surveys, local shoreline changes could be determined and quantified.

Data acquisition

During the field survey in August 2012, data was collected at the Border and Komakuk site (Figure 8) using either a Novatel (Antenna model: NOV702L_1.01) or Ashtech (Antenna model: ASH701975.01AGP) RTK-GPS at the Komakuk and Border study areas, respectively.

The advantage of an RTK-GPS is its high accuracy considered in coastal surveys to be about 5 cm both horizontally and vertically. This can be obtained due to the usage of the signal's carrier wave phase together with a stationary base receiver transmitting corrections and resolving phase ambiguities in real time, resulting in high position accuracy for the moving rover antenna (Sabatini & Plamerini 2008; Zinas 2011). In simplified terms, this means that satellite GPS signals (in the 2012 field survey from at least 10 satellites) are collected by the base station (Figure 9) and used for monitoring system errors. This information is used to send out correction data to the moving rover (Figure 10) where a recalculation of the measured data and thus a relocation of the current position takes place (NRCan 2009; GeoDZ 2010). For the 2012 field survey, an RTK-GPS with one base station was used. Since only relative point positions with reference to the base station can be determined with this measurement technique, knowing the exact position of the base station is crucial for accurate positioning of the measured points in a total reference system. Thus the base station was set above a ground control point (Komakuk site: GSC 336, Border site: CANUSA1, Figure 8, 9).

Consistent with previous GSC field surveys, beach, cliff and backshore profile data were acquired for each site. At the Border site, three out of three transect lines were resurveyed and at the Komakuk site, five out of nine existing transects were resurveyed. At the Komakuk site, data acquisition was limited due to time issues. Thus every second transect was walked down with the GPS antenna, starting at transect no. 1 (surveyed transects: 1, 3, 5, 7, 9). Transects for both study sites are shown in Figure 8. GPS data were collected at each point where there was a change in slope, sediment grain size, or vegetation. On the cliff slopes we chose survey points which adequately represented the cliff shape. In addition to the transect data, cliff toe and cliff top positions (Figure 10), as well as water level elevations were acquired by setting the GPS device to an auto-interval mode in which the GPS device automatically collected data every metre while walking the respective survey line. The water level data indicate the swash zone and thus the transition zone between water and land. As tides do not usually exceed 50 cm and calm wind conditions prevailed during and in advance of the survey period, no significant measurement distortions are expected as a result of water level anomalies. The cliff toe measurements indicate the transition from the beach to the cliff. East of the Komakuk landing strip where cliffs are very gentle and small, the vegetation line was additionally used to determine the cliff toe line. The cliff top data indicate cliff escarpments. Again, due to time constraints and problems with the equipment, water level elevations could not be acquired for the Border site, and could only be obtained for parts of the Komakuk study area.

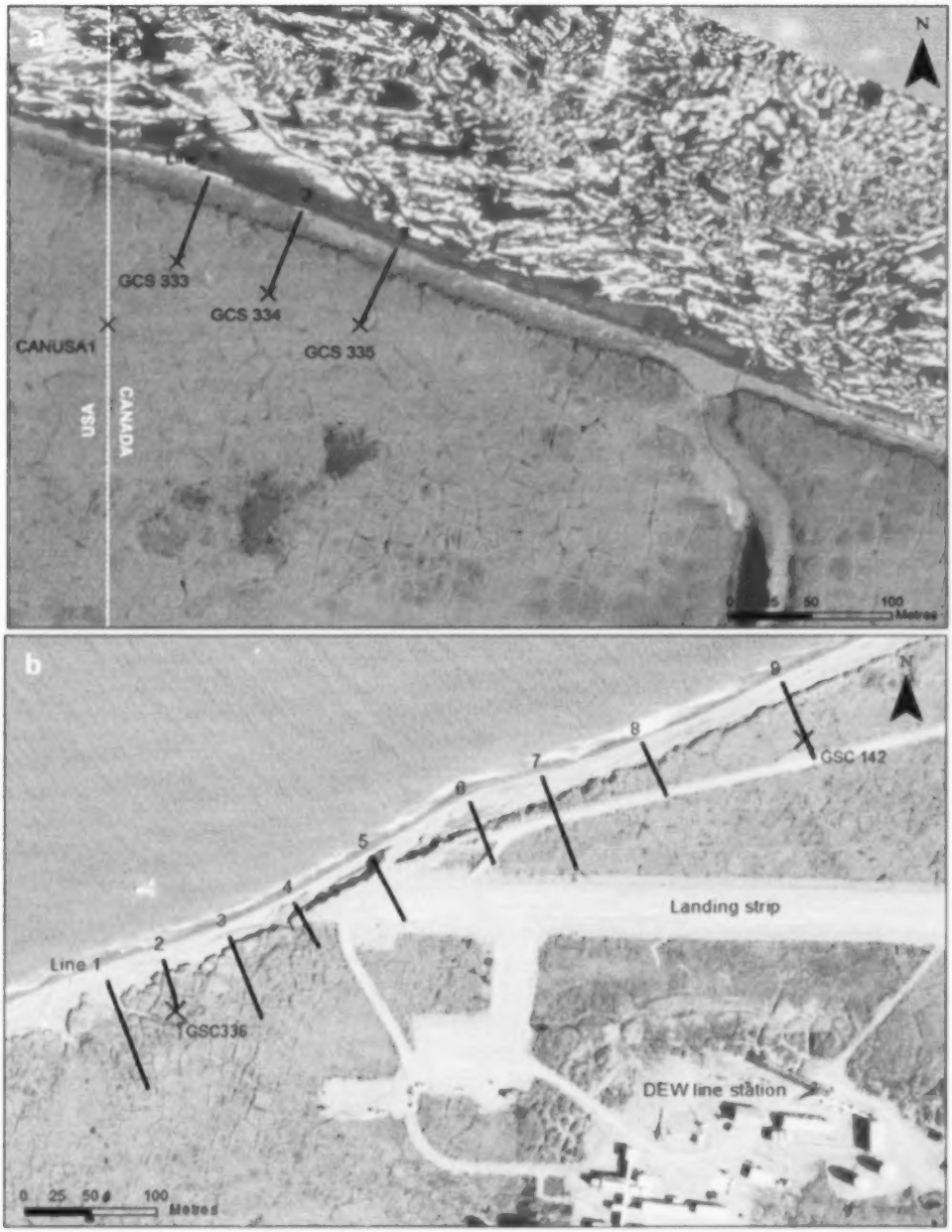

Figure 8: Positions of GPS transect lines. Black crosses indicate ground control points. a) Border study site. Transect spacing is roughly 60 m, and the total length of the investigation area amounts to approximately 120 m. Aerial photography is from 1994 and the border position was obtained from GeoBase Canada 2012. b) Komakuk study site. Transect spacing varies from 40 m between lines 1 and 2, to 120 m between line 8 and 9. The total length of the investigation area is roughly 570 m. Aerial photography is from 1992.

Figure 9: RTK-GPS base station setup at Komakuk site. GPS-antenna on top of tripod, radio transmitter (blue box) attached to tripod. Photo: A. Konopczak, 2012.

Figure 10: RTK-GPS measurement of cliff top position at Border site. GPS-antenna with handheld controller installed on yellow staff, radio antenna on top of back pack (blue cylinder). Photo: G. Manson, 2012.

Data preparation

After data acquisition was completed, in order to determine the most accurate position of the base station for both study sites, a post-processing of the base station's coordinates was conducted by means of the Canadian Service Reference System Precise Point Positioning (CSRS-PPP) service operated by the Canadian Geodetic Survey Division (GSD). After receiving the corrected coordinates, the difference between the original and corrected coordinates could be calculated and a 3D shift was applied to all Komakuk and Border survey data from 2012, by using the GSC-Atlantic RTK File Processor software

written in Visual Basic 6.0 by G. Manson in order to relocate the survey data to the correct absolute position. This process was repeated with the corrected base station coordinates for all data from previous surveys as well, so that a database of the highest possible accuracy was created for further use. In the case of the Tachymeter surveys, a manual recalculation of the data was carried out. A list of all data used for this study is shown in Table 2.

Table 2: GSC field survey data used for analyses.

Site	Year	Survey equipment	Accuracy	Surveyed lines
	1997	RTK-GPS	< 10 cm	4,6,8,9
Komakuk	2000	RTK-GPS	< 10 cm	2,3,4,6,7,8,9
	2003	RTK-GPS	< 10 cm	2,4,9
	2006	RTK-GPS	< 10 cm	1,2,3,4,5,6,7,8,9
	2012	RTK-GPS	< 10 cm	1,3,5,7,9
Border	1991	Tachymeter	sub-meter	1,2,3
	1999	RTK-GPS	< 10 cm	1,2,3
	2006	RTK-GPS	< 10 cm	1,2,3
	2012	RTK-GPS	< 10 cm	1,2,3

Data processing

As the field survey data only provide point position information and optionally typed in field notes, the data were used for the calculation of cliff position differences (E) between the survey years, average rates of shoreline change per year (E_{ave}), cliff slopes (C_{slope}), average cliff heights (C_{height}) and beach widths (B_{width}) (Figure 11).

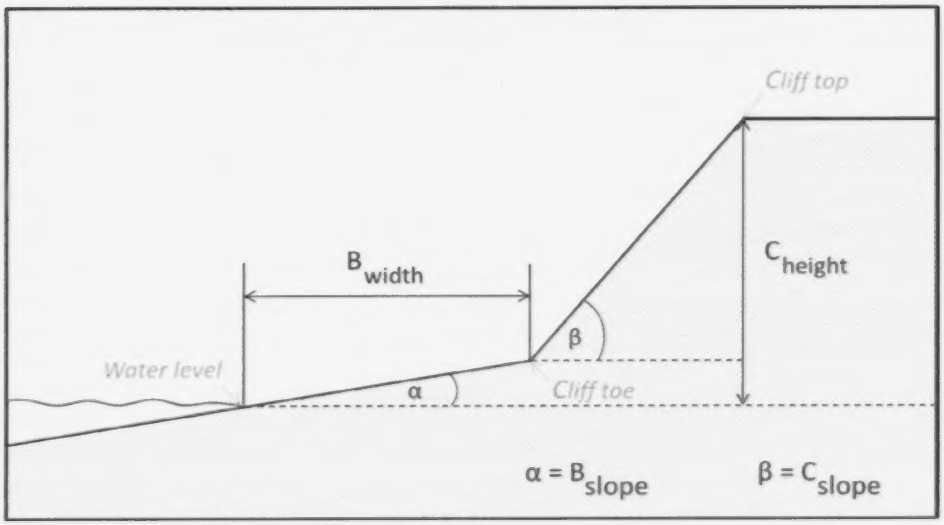

Figure 11: Schematic shoreface profile with the calculated parameters; beach width (B_{width}), beach slope (B_{slope}), cliff height (C_{height}), cliff slope (C_{slope}).

The cliff edge position differences (E) (in metres) were calculated as follows:

$$E = \sqrt{(\Delta x)^2 + (\Delta y)^2}. \quad (1)$$

The difference between the x or y coordinates of the younger and older cliff edge positions are expressed by Δx and Δy.

The average annual rate of change (E_{ave}) (in metres per year) was calculated by dividing the differences in cliff edge position by the time span of measurement Δa, i.e.

$$E_{ave} = \frac{\sqrt{(\Delta x)^2 + (\Delta y)^2}}{\Delta a}. \quad (2)$$

Mean beach widths (B_{width}) given in metre were calculated using the equation

$$B_{width} = \frac{\sum_{i=1}^{n} \sqrt{(\Delta a_i)^2 + (\Delta b_i)^2}}{n}. \quad (3)$$

The difference of the x and y coordinates of water level according to the Canadian Geodetical Vertical Datum 1928 (CGVD28) and cliff positions are given by Δa and Δb. In order to get an average beach width for one year, all results for each year were summed and divided by the number of calculations n.

Beach slopes (B_{slope}) were determined by calculating the horizontal distance between the cliff toe and water level position, and then dividing the height difference of these points Δz by their horizontal distance. The results represent beach slopes in degrees, i.e.

$$B_{slope} = \tan^{-1}\left(\frac{\Delta z}{\sqrt{(\Delta j)^2 + (\Delta k)^2}}\right). \quad (4)$$

Average cliff heights in metre (C_{height}) for each study site were determined by adding cliff edge heights and dividing them by the number of measurements n, i.e.

$$C_{height} = \frac{\sum_{i=1}^{n} h_i}{n}. \quad (5)$$

Cliff slopes (C_{slope}) were determined by calculating the horizontal distance between the cliff edge and cliff toe position, and then dividing the height difference of these points Δz by their horizontal distance. The results represent cliff slopes in degrees, i.e.

$$C_{slope} = \tan^{-1}\left(\frac{\Delta z}{\sqrt{(\Delta p)^2 + (\Delta q)^2}}\right). \quad (6)$$

A visualization of cliff profile evolution over time was done using Grapher software. No cliff profile could be drawn for transect number 4 at the Komakuk site because of a lack of an appropriate number of representative points.

After calculating all parameters, single and multiple linear regression analyses using the least squares technique were calculated in order to determine the degree of correlation between the dependent attribute (u) which is given by (E_{ave}) and the independent attributes (v) which are given by (B_{width}), (B_{slope}), (C_{height}) and (C_{slope}). For the single regression analyses, the empirical correlation coefficient ($Corr_e$ (u,v)) was calculated as follows:

$$Corr_e(u,v) = \frac{\sum_{i=1}^{n}(u_i-\bar{u})(v_i-\bar{v})}{\sqrt{\sum_{i=1}^{n}(u_i-\bar{u})^2 \sum_{i=1}^{n}(v_i-\bar{v})^2}}. \quad (7)$$

The multi-linear regression was calculated using the following equation:

$$\beta = \frac{\sum_{i=1}^{n}(u_i-\bar{u})(v_i-\bar{v})}{\sum_{i=1}^{n}(u_i-\bar{u})^2}. \quad (8)$$

In both formulas u and v represent attributes and $\bar{u}$ and $\bar{v}$ constitute the empirical means ($\bar{u} = \frac{1}{n}\sum_{i=1}^{n} u_i$ and $\bar{v} = \frac{1}{n}\sum_{i=1}^{n} v_i$). $Corr_e$ (u,v) is a dimensionless coefficient ranging from -1 (full negative correlation) to 1 (full positive correlation), whereas the value of 0 implies, that no linear correlation exists between the two attributes u and v (Arens et al. 2010).

The coefficient of determination (r^2) describes how well the independent attributes describe the variability of the dependent attribute. The coefficient ranges from 0 (the regression line does not fit the data set at all) to 1 (the regression line matches perfectly with the data set) (Arens et al. 2010). The r^2 values are calculated as follows:

$$r^2 = \frac{\sum_{i=1}^{n}(v_i-\hat{v}_i)^2}{\sum_{i=1}^{n}(v_i-\bar{v}_i)^2}. \quad (9)$$

In the upper part of the equation, the variation of the residuals is calculated, and in the lower part, the variation of the independent attribute.

All calculations were performed for the Border and Komakuk site as a whole, and additionally for each of the three sectors of the Komakuk site (Figure 5).

Remote sensing data

Remote sensing data consisting of historical aerial photography and more recent satellite imagery can be used to extend the shoreline change rates derived from ground surveys back in time and over longer lengths of coast. Aerial photographs were acquired, scanned, and georeferenced. Shorelines were digitized and analyzed with the Digital Shoreline Analysis System (DSAS) extension version 4.3 for Esri ArcMap which calculates rate of change statistics such as end point rates or linear regression rates of shoreline positions from different years. These processing steps are further described in the following sections.

Data acquisition

The predominant remote sensing imagery available is vertical aerial photographs collected from an aircraft. Although this method has been broadly applied since the late 1920's, photos from the study area only exist for the time period from 1951 to 1994. These were found by the means of the online search application of the National Air Photo Library (NAPL) which is in charge of all federal non-military aerial photography (NAPL 2007, NAPL 2010). As the online search function only indicates the approximate location of a given picture, all aerial photographs which potentially display the investigation area were determined. The local air photo archive of the GSC-Atlantic office was systematically searched for these photos and any photos not in the existing archive and determined to be especially valuable were ordered from NAPL. As the Komakuk site with its DEW line station was of particular interest for the American and Canadian governments, aerial photography was flown more frequently at this site than at the Border site and more photos were available. Table 3 shows all the photos that were acquired.

All aerial photos were then scanned with a dots per inch (dpi) number resulting in sub-metre pixel resolution ranging from 0.21 m to 0.76 m. This does not necessarily mean that objects of sub-metre size are clearly distinguishable, as the scale of the pictures is coarse, ranging from 1:5000 to 1:70000. One image acquired from a colleague rather than from the archives was received at a ground resolution of 2.45 m. Appendix II lists all used photos with their corresponding scale, scanned dpi number and resulting image resolution.

Table 3: Acquired and used aerial photography data.

Site	Year	Available photos	Used photos	Site	Year	Available photos	Used photos
Komakuk	1951	1	1	Border	1951	1	1
	1964	4	3		1972	1	1
	1971	6	0		1976	1	1
	1972	2	2		1992	6	1
	1975	8	4		1994	5	5
	1976	1	0		**Total**	**14**	**9 (64%)**
	1984	8	4	In between	1951	2	2
	1992	8	7		1972	2	2
	1993	3	3		1992	9	6
	Total	**41**	**24 (58%)**		1993	6	3
					Total	**19**	**13 (68%)**

Data preparation

The preparation of scanned aerial photographs for running the DSAS extension requires four steps: image clipping, georeferencing/ co-registration, digitizing of shorelines, and creation of feature classes.

Image clipping

In remote sensing images, the 3-dimensional earth surface is projected onto a 2-dimensional surface, which, especially in aerial photographs, can result in geometric distortions and displacements. These errors can be caused by terrain relief, by the camera perspective, or by the motion and altitude of the aircraft, to name just a few (NRCan 2008; Paine & Kiser 2012). As all aerial photographs of the study area were imaged in central projection, the distortion increases with distance from the picture center. In order to prevent major errors resulting from distortions, 15-20% of each picture margin was clipped, thus leaving just the center extract for further use. This process resulted in data exclusion, as photographs which displayed the shoreline too close to the picture margins did not get processed for further use. Even though this meant a further limitation of an already limited amount of data (Table 3), the potential disadvantages resulting from the use of these pictures was estimated to be higher than the advantage of having a larger database.

Georeferencing / Co-registration

As the scanned and clipped pictures contained no spatial reference information, they needed to be georeferenced to an already aligned dataset and additionally co-registered to each other. This process was conducted using the georeferencing tool in ArcMap. Various georeferenced satellite images were considered as a base for this process. It was decided to use an image created using data acquired between 2005 and 2010 by the French satellite "*Satellite Pour l'Observation de la Terre*" (SPOT) 4 and 5 (CCOG 2013). The extent of the SPOT scene which covers the study area was acquired in 2009. Even if the SPOT image had the coarsest ground resolution of only 10 m (panchromatic band), at that time it was the only

available ortho-rectified image which covered the whole study area, so it was used in order to avoid adding up position uncertainties caused by distortion.
First, all Komakuk pictures were processed. The most recent dataset from 1993 was chosen to begin with, as it has the best quality and a very good ground resolution of 0.25 m. Another advantage for starting with this dataset was the fact that even after clipping the picture margins, there was still an overlap of approximately 40 to 50% between the pictures. Furthermore, as this was the most recent dataset, the differences between it and the SPOT image were assumed be the lowest. Because the Komakuk site contains some permanent structures such as buildings and a paved landing strip, the photo which showed these structures was the first to be georeferenced with the SPOT image. Similar objects were identified on both images and set in relation to each other by marking both spots with ground control points (GCP). After this, each consecutive air photo was co-registered to the former one using tie points (same process as georeferencing) and georeferenced to the SPOT image where no co-registration was possible. Initially, a simple co-registration of the images was tested, taking the middle picture as starting point. However, only part of the picture was co-registered and the other part was warped very strongly. Thus, it appeared to be a better method to georeference one part of the photo to the SPOT image, while co-registering the other half to the adjacent previously georeferenced photo.
Once the data from one time period were georeferenced, photos from the time period immediately prior were georeferenced to them, as well as co-registered to each other. However, when the coarse ground resolution of a dataset seemed to affect a successful georeferencing of the subsequent dataset, a dataset of higher quality was chosen for georeferencing. After the data processing for one year was finished, the photos were joined together to facilitate further use using the ArcMap 'mosaic' function. Appendix II provides an overview of all datasets and the specific mosaics which were used as their georeferencing base.
Except for those at the Komakuk site, no other structures exist within the study area, so stable natural features such as lake shorelines or ice wedge polygon intersections were used (MacKay 2000; Jones et al. 2008). Yet a reconsideration of the applicability of some of these features as a GCP was often required during the georeferencing process. Because of varying picture qualities or different (preceding) weather conditions and/or sun angles during overflight, not all features could be distinguished in all photos. This source of uncertainty is mitigated by conducting this work in the Arctic (beyond the tree line, with no high buildings) in that GCPs are far less influenced by position errors caused by distortion. Appendix II contains information about the number of GCPs used for the georeferencing of each picture. The high number of GCPs per image is explained by the large extent of some pictures and the fact that, besides a focus on the coast, the operator was also georeferencing the rest of the picture, thus providing a more accurate co-registration and georeferencing base for the following pictures. Despite the fact that a high number of GCPs can influence the result in a negative way, the number of GCPs is still considered as being necessary and constructive.
As in comparable studies conducted by Solomon (2004) and Mars & Houseknecht (2007), a 2nd-order polynomial transformation was applied in order to calculate the relocation of the aerial photography. The root mean square (RMS) of each picture was recorded and after referencing all photos for one year, an average RMS for the corresponding mosaic was calculated. Since the RMS indicates the average distance of the GCPs of the overlapping picture to the corresponding GCPs of the base picture, it is an indicator of reference-accuracy, but can also be negatively influenced by using more GCPs. For all mosaics, the mean RMS error was kept below 3 metres (Appendix II).
In order to expand the time frame and to set a reference to the present state of the coast, the SPOT scene from the end of July 2009 was also used in the DSAS analyses.

Creation of a DSAS database

Data preparation for DSAS requires four steps. First, a personal geodatabase is created; then feature classes are constructed (one for each shoreline and one for the baseline); and all shorelines and the baseline are digitized. Finally, shoreline pairs are compiled into new feature classes of which DSAS analyses were calculated (Figure 12). DSAS requires a specific data structure in order to run (Figure 12). A suitable geodatabase conforming to DSAS requirements was created in ArcCatalog. The type of geodatabase is predefined to be a personal geodatabase and cannot be modified. Next, feature classes for

the baseline and each shoreline were created according to the special attribute table requirements of the DSAS tool (more detailed information about attribute table settings can be obtained from the DSAS manual guide (Thieler et al. 2009). Usually only one feature class for all shorelines is required, but because a number of different analyses had to be conducted within the framework of this thesis, each shoreline was defined as a single feature class.
The baseline was developed from the most recent shoreline position (SPOT 2009 image) in order to make sure that the baseline lies on the landward side of all shorelines. This facilitates the subsequent DSAS calculations. All shorelines were digitized on screen at an initial scale of 1:800, though it was sometimes required to zoom in up to a scale of 1:200.
Different indicators can be used for the shoreline when digitizing, such as for example the wet/dry line or the high water line (Boak & Turner 2005). Here, the cliff edge was used for shoreline determination, since the small beaches fronting the cliffs often are not clearly distinguishable, thus hampering shoreline detection. In non-cliff or gentle cliff areas, such as Clarence Lagoon, the vegetation line was taken as the shoreline indicator, or if not present, the darker part of the beach, indicating driftwood accumulation.
Since DSAS offers additional analyses which include shoreline position uncertainties, these uncertainties were added to the attribute table. Because the cliff edge in treeless environments is relatively easy to determine, shoreline uncertainties resulted mainly from different photo resolutions. Shoreline uncertainties were determined for the larger scale and local position inaccuracies were disregarded, as in this work DSAS analyses are used to provide measure of the overall coast's dynamics.
After all shorelines were digitized, a feature class was created for each shoreline combination from which a DSAS analysis was desired, by copying the shorelines and adding them to the respective new feature classes. This was necessary since DSAS computes overall statistics, without providing results of interim steps. That means that if DSAS computes shoreline statistics for a feature class which contains shorelines from four different years, the result table only provides information about the overall statistics, for example the overall net shoreline movement (NSM) from the entire four year period. But if the temporal dynamics of the NSM are of interest, the NSM of each one-year time step needs to be calculated. The easiest way to do this is to use DSAS to calculate separate statistics for each time period which is why the extra feature classes were created.

Functionality of the DSAS tool

In order to understand the data processing steps, it is helpful to know how the tool works. DSAS creates transects from the baseline perpendicular to the shorelines and uses the intersection points and the information contained in the shoreline attribute table to calculate rate of change statistics. The creation of transects and the calculation of statistics are separate steps which allows the operator to optimize the results by modifying transect and/or baseline positions before the statistics are calculated (Thieler et al. 2009). As the calculated statistics are only as reliable as the shoreline position data, special statistics are calculated for shorelines with varying position uncertainties. Therefore the shoreline's position uncertainty has to be entered in metres in the attribute table and should account for both measurement and positional uncertainties. The uncertainty value is included in the calculation of the weighted linear regression statistic, as well as its supplemental statistics (Thieler et al. 2009).

Data processing

All data processing steps are illustrated in Figure 12.
Step 1: Set default parameters
First, all prepared feature classes (shoreline feature class, baseline feature class) were added to ArcMap and some general settings were made. These mainly consist of defining the baseline and shoreline layers, entering the desired transect spacing (set to 50 m for this study), entering a default shoreline uncertainty (the value did not matter here because all shorelines had an entered uncertainty value), choosing an intersection parameter (set to closest intersection), and providing metadata information about the project and the operator. The transect spacing was set to 50 m, as this distance seemed to be convenient for capturing changes in shoreline evolution without missing crucial information.

Step 2: Cast transects

The second step is to define settings for the transects that are cast from the baseline to intersect the shorelines. The default cast settings were kept (smoothed baseline, smoothing distance: 50 m). As these settings define the location of transects in curved baseline sections, they were irrelevant for this work, since the baseline is straight with no abrupt curves. After these settings were added, the transect layer was created.

Step 3: Edit

After the transect layer was created, it was manually edited to correct places where transects ran through river deltas, channels or gullies. Depending on the position of the transect and the width of the channel or gully, they were either deleted or relocated to an adjacent even stretch of shoreline. Transects crossing river deltas were deleted. These manual edits of the transect layer were done in order to prevent result distortions, since shoreline detection in gullies or delta channels could not be done consistently, especially because of shadow effects and the lack of an appropriate shoreline indicator within these features. After editing, the transect layer contained a total of 638 transects. Twenty one of these (transects 2 to 22), spanning a length of 1050 m, were used in calculations for the Komakuk site, while 48 (transects 589-653), spanning a length of 2400 m were used for the Border site calculations. The boundaries of both study sites were determined by the mosaic which covered the smallest extent of the study area. Thus, shoreline change analyses for all years could be compared on a common basis. Since the spatial coverage of the imagery was very extensive for the Border site, the morphology of the cliffs was also taken into consideration so that it was the area with excessive thermal denudation (Figure 3) that determined the boundary of the site.

Step 4: Calculate change statistics

The same set of transects was used for all calculations in order to guarantee similar conditions for all analyses and to establish a basis for comparison of all results. After selecting the transect layer, the desired output statistics were selected. Two different circumstances were of interest for each of the local study sites and for the overall area. The first was the change of the coast for each area from one time period to the next, involving only two shorelines at a time; the other circumstance was the overall survey of each area for the entire time span, so all available shorelines were included. For the change from one time period to the next, only net shoreline movement, end point rate and least median of squares values were calculated, For the overall survey, all statistics were calculated, so linear and weighted regression rates and their supplemental statistics were included as well. Where the calculations included numerous shorelines, the shoreline intersection threshold was set to the number of used shorelines, thus guaranteeing that all shoreline positions were integrated into the analyses. The confidence interval describes in which range a certain percentage of all data is situated. It was set to 95%, as this number was considered as being a meaningful indicator for the distribution of the data.

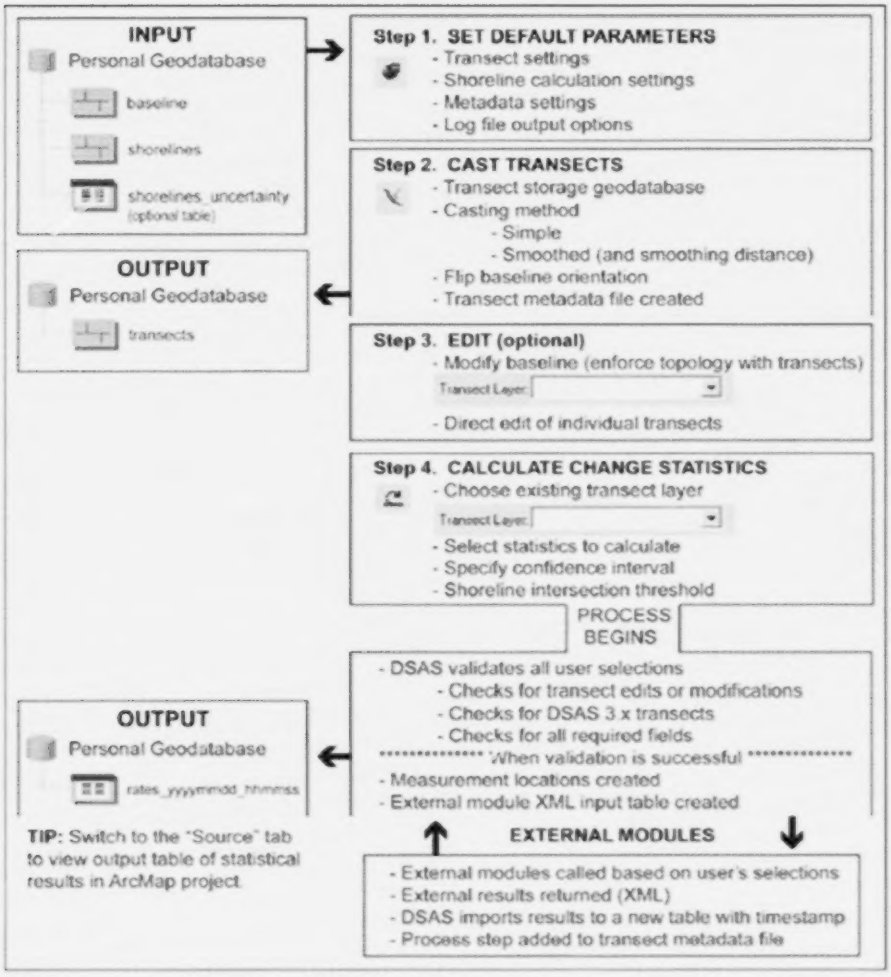
INPUT
Personal Geodatabase
baseline
shorelines
shorelines_uncertainty
(optional table)
OUTPUT
Personal Geodatabase
transects
Step 1. SET DEFAULT PARAMETERS
- Transect settings
- Shoreline calculation settings
- Metadata settings
- Log file output options
Step 2. CAST TRANSECTS
- Transect storage geodatabase
- Casting method
- Simple
- Smoothed (and smoothing distance)
- Flip baseline orientation
- Transect metadata file created
Step 3. EDIT (optional)
- Modify baseline (enforce topology with transects)
Transect Layer:
- Direct edit of individual transects
Step 4. CALCULATE CHANGE STATISTICS
- Choose existing transect layer
Transect Layer:
- Select statistics to calculate
- Specify confidence interval
- Shoreline intersection threshold
PROCESS BEGINS
- DSAS validates all user selections
- Checks for transect edits or modifications
- Checks for DSAS 3.x transects
- Checks for all required fields
When validation is successful
- Measurement locations created
- External module XML input table created
OUTPUT
Personal Geodatabase
rates_yyyymmdd_hhmmss
TIP: Switch to the "Source" tab to view output table of statistical results in ArcMap project.
EXTERNAL MODULES
- External modules called based on user's selections
- External results returned (XML)
- DSAS imports results to a new table with timestamp
- Process step added to transect metadata file

Figure 12: Steps of use of the DSAS tool (Thieler et al. 2009).

DSAS statistics

DSAS provides six different primary statistics and several more supplemental ones (Table 4). The net shoreline movement (NSM) and the shoreline change envelope (SCE) represent statistics of total changes in shoreline position, whereas the linear regression rate (LRR), the weighted linear regression rate (WLR) and the least median of squares (LMS) represent annual rates of change, all based on linear regression. In the calculation of the LRR, a regression line is calculated through the intersection points of the respective transect, and its slope constitutes the rate of change. The WLR statistic follows the same principle whereby the regression line is calculated with respect to the provided shoreline uncertainties, since intersection points with higher uncertainties are weighted less than more accurate ones. In comparison to the LRR and WLR statistics which calculate a line which minimizes the sums of the squared residuals, the LMS method calculates a line which minimizes the median value of the sums of all squared residuals, thus paying less attention to outliers (Thieler et al. 2009).

The end point rate (EPR) is another statistic which is based on the net shoreline movement, but divided by the number of years under consideration, thus also representing an annual rate of change. A supplemental statistic for the confidence of the end point rate (ECI) is also provided. The linear regression rate and the weighted linear regression rate have supplemental statistics which provide additional information about the accuracy and thus reliability of the statistical outputs; these include the standard errors (LSE/WSE), the confidence intervals (LCI/WCI) of the percentage which has been chosen under the "calculate statistics" button (in this case 95%), and the r-squared values (LR2/WR2). The LSE and WSE values give the average distance in metres of the estimated to the actual value. The LCI and WCI outputs describe the uncertainty of the reported rate. For example, if a 95% confidence range is chosen, the LCI/WCI output ± the reported rate of change describes the range in which one can be 95% confident that the true rate of change lies, leaving a 5% uncertainty that the true rate of change lies outside this range. The LR2/WR2 value describes how well the variance in the data can be explained by a regression, with a value of 0 implying that the regression line explains no variation in the dependent variable, and a value of 1 indicating that all variations in the dependent variable can be explained by the regression line (Thieler et al. 2009).

Table 4: DSAS statistical outputs (Thieler et al. 2009).

	Main statistics	**Supplemental statistics**	
NSM	Net shoreline movement		
SCE	Shoreline change envelope		
EPR	End point rate	ECI	Confidence interval of end point rate
LRR	Linear regression rate	LSE	Standard error of linear regression
		LCI	Confidence interval of linear regression
		LR2	R-squared of linear regression
WLR	Weighted linear regression rate	WSE	Standard error of weighted linear regression
		WCI	Confidence interval of weighted linear regression
		WR2	R-squared of weighted linear regression
LMS	Least median of squares		

Calculation of total land loss

In addition to calculating changes in shoreline position, the shoreline feature classes from 1951 and 2009 were used for the calculation of the total area of land loss for the entire coastline. A polygon shape file was created using the shorelines to define the extents, and a calculation of the area of the polygon was run with ArcMap field calculator. In order to be able to give an estimate about the total volume loss in m^3,

cliff heights for the entire coast were estimated from a 1999 GSC aerial video survey, by using heights from the 2012 survey and 2012 LIDAR data as reference. After adding the respective cliff heights to the attribute table, total volumetric land loss was calculated using the ArcMap field calculator.

Results

According to the two different databases, first the GPS results obtained from the field surveys are presented, followed by the DSAS analysis results obtained from the remote sensing data. In the last section the results of the total land loss calculation are presented.

GPS surveys

GPS surveys covering a total time span of 21 years for the Border site and up to 15 years for the Komakuk site were analyzed to determine changes in shoreline positions and shore profiles.

Border site erosion rates

Shoreline recession was examined both spatially and temporally, and calculations were based on changes in the cliff edge measurements. For the Border site, NSM was highest at line 2 with a total retreat of 26.28 m over the 21 years, whereas the smallest cumulative shoreline retreat was at line 3 with 20.14 m. Erosion rates ranged from -0.87 m/a to -1.54 m/a with an overall mean of -1.13 m/a ± 0.18 m/a (Table 5). Erosion rates showed the highest variation at line 2 with a difference of 22.31% from the mean erosion rate per time period and were most consistent at line 1. Additionally, the mean annual erosion value for each survey line was calculated. The rates were 1.14 m/a, 1.25 m/a and 0.96 m/a for line 1, 2 and 3, respectively (Table 5). The largest variance between the overall mean erosion rate and a mean line erosion rate was 18.13% for line 3 which had the lowest erosion rates (Table 6). Annual erosion rates calculated for line 1 are very consistent through time and reveal the smallest variance from the overall mean erosion rate, amounting to 0.52%.

Annual erosion rates were highest in the first time period from 1991 to 1999, with a mean of 1.26 m/a, and decreased in each subsequent period, leading to an overall decrease of 15.87% over the 21 years of measurement (Table 5). Variation between the overall mean erosion rate and the mean erosion rate for each time period was highest for 2006 to 2012, amounting to a decrease of 10.27%. The highest variation between a single erosion rate and the mean rate for one time period occurred at line 2 and was 22.31% for the time period from 1991 to 1999.

In summary, the analyses of the GPS survey data show that, at the Border, site spatial changes in the shoreline have a higher variability than temporal changes in shoreline recession over the 21 year period of measurement.

Table 5: Results for erosion calculations of the Border site. NSM is the net shoreline movement, ER is the erosion rate, σ is the standard deviation. Negative variation which shows a decrease in the erosion rate from the mean is indicated by ↓.

Line no.	Time period	Mean NSM [m]	Mean ER [m/a]	Mean ER per line [m/a]	Variation btw. mean ER and mean line ER [%]	Mean ER for all lines per time period [m/a]	Variation btw. mean ER and mean ER per time period [%]
1	1991-1999	-9.15	-1.14	-1.14	0.57	-1.26	↓9.27
	1999-2006	-8.16	-1.17		2.56	-1.08	7.94
	2006-2012	-6.57	-1.09		↓3.72	-1.06	3.24
2	1991-1999	-10.79	-1.54	-1.25	23.26		22.31
	1999-2006	-8.43	-1.20		↓3.68		11.50
	2006-2012	-7.06	-1.18		↓5.94		10.95
3	1991-1999	-8.65	-1.08	-0.96	13.03		↓14.14
	1999-2006	-6.07	-0.87		↓9.43		↓19.73
	2006-2012	-5.42	-0.90		↓5.70		↓14.85
Overall mean ER [m/a] ± σ				-1.13 ± 0.18			

Table 6: Mean erosion rates for each line at the Border site. ER is the erosion rate, σ is the standard deviation. Variation which shows a decrease in the erosion rate from the mean is indicated by ↓.

Line no.	Mean ER [m/a]	Variation btw. mean ER and overall mean ER [%]
1	-1.14	0.52
2	-1.25	9.57
3	-0.96	↓18.13
Overall mean ER [m/a] ± σ	-1.13 ± 0.18	

Table 7: Mean erosion rate for all lines for each time period at the Border site. ER is the erosion rate, σ is the standard deviation. Variation which shows a decrease in the erosion rate from the mean is indicated by ↓.

Time period	Mean ER [m/a]	Variation btw. mean ER and overall mean ER [%]
1991-1999	-1.26	10.27
1999-2006	-1.08	↓4.69
2006-2012	-1.06	↓6.67
Overall mean ER [m/a] ± σ	-1.13 ± 0.18	

Border site shore profiles

Cross shore profiles based on GPS measurements show shore profile changes through time (Figure 13). The plots for each GPS transect do not show significant changes with time or between survey lines, indicating that cliff retreat occurs mostly uniformly. Evidence for this observation is also given by the low standard deviation of the overall mean annual erosion rate of 0.18 m/a discussed in the previous section (Table 7).

Calculations based on GPS values provide better temporal resolution data as the DSAS results. Table 8 displays all calculations, averaged for each survey line and time period. The averaging was necessary in order to determine correlations between the calculated shore profile measures (i.e. beach width, beach slope, absolute cliff height, relative cliff height) and mean annual erosion rates. Appendix III displays the scatter plot for each shore profile parameter.

The beach width was calculated with reference to the Canadian Geodetic Vertical Datum from 1928 (CGVD28). It was lowest in between 1999 and 2006 at line 1 (11.20 m) and widest in between 2006 and 2012 at line 3 (19.96 m). The correlation between beach widths and mean erosion rates is very strong ($r=0.84$) and statistically significant at $\alpha=0.05$. The lowest beach slope was calculated for line 3 (2006-2012) with 4°, and the steepest beach slope was measured at line 2 (2006-2012) with 6°. The correlation of beach slopes with the mean erosion rates reveals a weakly negative correlation of -0.34 and no statistical significance. The negative sign implies that the erosion rates are when the beach is steeper.

The absolute cliff height represents the elevation of the cliff top with reference to CGVD28, whereas the relative cliff height is the height difference between the cliff top and the cliff toe. Absolute cliff height values range from 5.22 m (line 2, 2006-2012) to 5.71 m (line 3, 1999-2006). Relative cliff heights are lower, with the lowest being 4.19 m at line 2 (1999-2006) and the highest amounting to 4.68 m at line 1 between 2006 and 2012. The absolute cliff height correlates strongly with mean erosion ($r=0.70$), whereas the relative cliff height only shows a very weak correlation ($r=0.19$). The correlations of both measures are not statistically significant.

The mean cliff slope, calculated from cliff top and cliff toe values, is steepest at line 3 for the time period of 2006 to 2012 with a value of 34.25°. The lowest cliff slope, (28.16°) was calculated for line 1 for the time period between 2006 and 2012. Cliff slope values correlate weakly with mean annual erosion rates ($r=0.34$) and the correlation is not statistically significant.

A multiple regression analysis was performed in order to determine how well the two parameters which show the highest correlation with mean erosion rates are able to explain the variation of erosion. The calculated r^2 which considers beach width and absolute cliff height amounted to 0.72.

In summary, at the Border site, mean annual erosion rate is significantly correlated with beach width, there is a compelling but insignificant correlation with absolute cliff height. The remaining shore profile components do not show correlation with mean annual erosion rates.

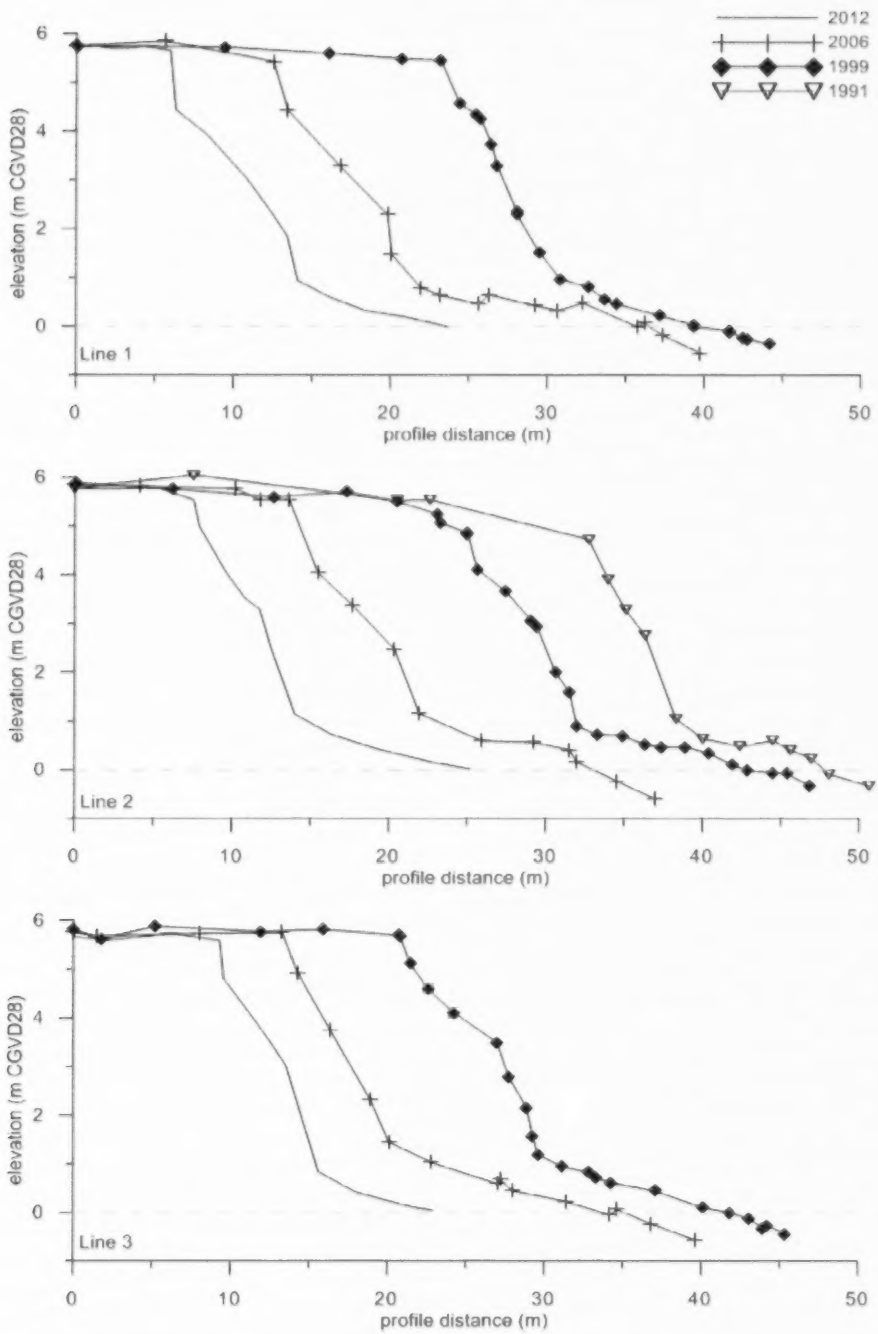

Figure 13: Shore profiles for the Border site generated from GPS measurements. CGVD28 is the Canadian Geodetic Vertical Datum 1928. For transect position see Figure 8.

Table 8: Mean shoreface profile statistics and correlation of each factor with erosion rate for the Border site. ER is the erosion rate, r is the correlation coefficient.

Line no.	Time period	Beach width [m]	Beach slope [deg]	Abs. cliff height [m]	Rel. cliff height [m]	Cliff slope [deg]	Mean ER [m/a]
1	1999-2006	11.20	5	5.45	4.57	28	-1.17
	2006-2012	11.73	4	5.54	4.68	28	-1.09
2	1999-2006	10.80	5	5.22	4.19	28	-1.20
	2006-2012	10.95	6	5.54	4.39	31	-1.18
3	1999-2006	15.33	5	5.71	4.39	29	-0.87
	2006-2012	19.96	4	5.67	4.52	34	-0.90
r		0.84	-0.31	0.70	0.19	0.34	/
Significant at α=0.05		Yes	No	No	No	No	/

Komakuk site erosion rates

The Komakuk site is a comparatively large survey site, so that no full investigation of all nine survey lines was conducted in any single year, except for 2006. Consequently, a comparison of the different erosion rates proves difficult. For consistency, it would have been best to just compare survey lines from the same time periods, however, this would further diminish the already limited data set. Therefore, it was decided to include all available data, keeping in mind that some erosion rates are calculated from different data sets. All available data for each line are listed in Table 3.

At the Komakuk site, shoreline recession rates range from -0.16 m/a (line 6, 1997-2000) to -3.45 m/a (line 9, 1997-2000), with an overall mean erosion rate of 1.14 m/a, which is very similar to the average annual Border site erosion (Table 9). The high variability in shoreline change is shown by a considerably high standard deviation of 0.80 m/a. This can be attributed to the fact that the data series includes some outliers. Of 24 calculated erosion rates, three are higher than 2 m/a and four are lower than 0.5 m/a, thus weighting the statistics and significantly increasing the standard deviation (Table 9). Consequently, the overall mean annual erosion rate does not appear to be an adequate reflection of coastal recession for this site.

Like at the Border site, the mean annual erosion rate was highest during the time period from 1997 to 2000, amounting to -1.77 m/a (Table 12), and decreased thereafter. In the three subsequent time periods, 2000 to 2003, 2003 to 2006, and 2006 to 2012, the annual erosion decreased from -1.29 m/a, to -0.89 m/a, to -0.77 m/a, respectively. This amounts to a total decrease in the erosion rate of 32.46% over 15 years. Rates for individual time periods vary greatly in comparison to the overall mean annual erosion rate, as seen in the 1997-2000 time period when the mean annual rate was 56.16% higher than the overall mean, and in the 2006-2012 period when the mean annual rate was lower than the overall mean by 32.39%.

Calculated by survey line, line 4 has the highest annual mean erosion rate with 1.38 m/a, amounting to a net shoreline movement of -12.72 m (1997-2006). The lowest mean annual erosion rate was recorded at line 7 with a value of -0.54 m/a, thus varying by 52.53% from the overall mean erosion rate (Table 10) and amounting to a net shoreline movement of -6.86 m. At 8 of the 9 survey lines, the mean annual erosion rate is lower than the overall mean annual erosion rate for the entire site.

As the Komakuk site has a very heterogeneous coastline, the shoreline was subdivided into three morphological sections (Figure 5; first section: lines 1 to 3; second section: lines 4 to 6; third section:

lines 7 to 9) and additional calculations were carried out for each section. Results show that the westernmost section (lines 1-3) is eroding at a rate which is comparable to the Border site, with a mean of -1.21 m/a, and that the rate has a standard deviation of 0.40 m/a (Table 11). The mean annual erosion rate of the second section (lines 4-6) is considerably lower at -0.95 ± 0.83 m/a. The mean annual erosion rate of the easternmost section (lines 7-9) is comparable to the first section, with a value of -1.24 ± 0.91 m/a, although the standard deviation is considerably higher than the one of section 1 amounting to 0.04 m/a (Table 11).

In summary, the analysis of GPS survey data show that at the Komakuk site temporal changes in shoreline recession are slightly higher than spatial changes. A comparison of shoreline change variability at both study sites shows that spatial as well as temporal variability of erosion at the Komakuk site by far exceeds the variances calculated for the Border site.

Table 9: Results for erosion value calculations of the Komakuk site. NSM is the net shoreline movement, ER is the erosion rate. Negative variation which means a lowering in the erosion rate is indicated by ↓. Positive variation (increase in erosion rate) is not indicated.

Line no.	Time period	Mean NSM [m]	Mean ER [m/a]	Mean ER per line [m/a]	Variation btw. mean ER and mean line ER [%]	Mean ER for all lines per time period [m/a]	Variation btw. mean ER and mean ER per time period [%]
1	2006-2012	-6.02	-1.00	-1.00	0	-0.77	30.24
2	2000-2003	-5.52	-1.84	-0.71	158.77	-1.29	42.74
	2003-2006	-1.55	-0.52		↓27.16	-0.89	↓59.82
3	2000-2003	-3.80	-1.27	-0.96	32.29		↓1.77
	2003-2006	-4.30	-1.43		49.65		60.66
	2006-2012	-7.21	-1.20		25.46		56.01
4	1997-2000	-8.77	-2.92	-1.38	111.72	-1.77	64.71
	2000-2003	-2.99	-1.00		↓27.76		↓22.68
	2003-2006	-0.96	-0.32		↓76.71		↓63.96
5	2000-2006	-5.23	-0.87	-0.72	21.81	-0.88	↓0.88
	2006-2012	-3.38	-0.56		↓21.35		↓26.86
6	1997-2000	-0.48	-0.16	-0.73	↓78.35		↓91.04
	2000-2006	-8.21	-1.37		86.43		55.51
	2006-2012	-2.41	-0.40		↓45.17		↓47.73
7	2000-2003	-2.13	-0.71	-0.54	31.79		↓44.87
	2003-2006	-3.26	-1.09		101.40		21.80
	2006-2012	-1.47	-0.24		↓54.61		↓68.20

8	1997-2000	-1.70	-0.57	-0.67	↓14.77		↓68.05
	2000-2003	-1.96	-0.65		↓1.86		↓49.39
	2003-2006	-3.86	-1.29		93.61		44.36
9	1997-2000	-10.35	-3.45	-0.92	275.52		94.39
	2000-2003	-6.81	-2.27		147.08		75.97
	2003-2006	-2.12	-0.71		↓23.22		↓20.94
	2006-2012	-8.58	-1.43		55.61		85.61
Overall mean ER [m/a] ± σ			-1.14 ± 0.80				

Table 10: Mean erosion rates for each line at the Komakuk site. ER is the erosion rate, σ is the standard deviation. Variation which shows a decrease in the erosion rate from the mean is indicated by ↓.

Line no.	Mean ER [m/a]	Variation btw. mean ER and overall mean ER [%]
1	-1.00	↓11.74
2	-0.71	↓37.40
3	-0.96	↓15.73
4	-1.38	21.48
5	-0.72	↓36.98
6	-0.73	↓35.40
7	-0.54	↓52.53
8	-0.67	↓41.47
9	-0.92	↓19.17
Overall mean ER [m/a] ± σ	-1.14 ± 0.80	

Table 11: Mean erosion rates for each section at the Komakuk site. ER is the erosion rate. Negative variation which means a lowering in the erosion rate is indicated by ↓. Positive variation (increase in erosion rate) is not indicated.

Line no.	Time period	Mean ER [m/a]	Mean ER for each section [m/a]	Variation btw. mean ER for each section and time period and mean ER for each section [%]
1-3	2000-2003	-1.55	-1.21 ± 0.40	↓28.36
	2003-2006	-0.98		19.41
	2000-2006	-0.68		43.43
	2006-2012	-1.10		8.95
4-6	1997-2000	-1.54	-0.95 ± 0.83	↓62.04
	2000-2003	-1.00		↓4.87
	2003-2006	-0.32		66.19
	2000-2006	-0.96		↓0.51
	2006-2012	-0.48		49.22
7-9	1997-2000	-1.80	-1.24 ± 0.91	↓45.46
	2000-2003	-1.21		2.36
	2003-2006	-0.81		34.30
	2000-2006	-0.91		26.92
	2006-2012	-0.92		26.15
Overall mean ER [m/a] ± σ		-1.14 ± 0.80		

Table 12: Mean erosion rate for all lines for each time period at the Komakuk site. ER is the erosion rate, σ is the standard deviation. Variation which shows a decrease in the erosion rate from the mean is indicated by ↓.

Time period	Mean ER [m/a]	Variation btw. mean ER and overall mean ER [%]
1997-2000	-1.77	56.15
2000-2003	-1.29	13.49
2003-2006	-0.89	↓21.50
2000-2006	-0.88	↓22.84
2006-2012	-0.77	↓32.39
Overall mean ER [m/a] ± σ	-1.14 ± 0.80	

Komakuk site shore profiles

The GPS transect plots provide a visual representation of the three morphological sections at the Komakuk site; west of the airstrip, at the airstrip and east of the airstrip (Figure 5). Line number 4 could not be depicted because of an insufficient number of GPS survey points across the profile. Lines 1 to 3, which mark the area west of the airstrip, show a low cliff which gets steeper to the east. Line 5, with a steep high cliff, can be clearly seen to form part of the airstrip. Line 6 is part of the adjacent eroding track. Lines 7 to 9 do not show a clear and consistent shore profile behavior and vary in beach height, in particular.

Calculations of mean shore profile values for each line and time period show much higher variations in between lines and time periods than at the Border site (Table 13, for scatter plots see Appendix IV). Beach widths vary considerably between 3.70 m (line 3, 2000-2006) and 33.37 m (line 6, 2000-2006). The values only show a weak correlation of 0.24 with the mean annual erosion rates and no statistical significance (α=0.05).

Steepest mean beach slope was calculated for the survey line with the narrowest beach (line 3), and amounted to 12° (2006-2012), whereas the lowest beach slope came to 1° and was calculated for line 7 (2000-2006). No correlation and no statistical significance were determined between beach slope and mean annual erosion rates (correlation coefficient of -0.04).

As can be seen in Figure 14, relative and absolute cliff heights are highest at the airstrip, measuring 4.81 m (2006-2012) and 6.51 m (2006-2012), respectively. The lowest absolute cliff height was calculated for line 9 (2000-2003) with a value of 2.92 m, whereas the lowest relative cliff height was calculated for line 2, with a value of 1.14 m (2003-2006). There is a tendency for cliff heights to increase from lines 1 to 5 and to decrease from lines 5 to line 9. Both, relative and absolute cliff heights correlate weakly with mean annual erosion rates of 0.23 and 0.34, respectively. No statistical significance was determined. Cliff slopes vary considerably from 6° (line 9, 2000-2003) to 48° (line 3, 2006-2012), whereas the calculation of the mean cliff slope for the preceding time period (2000-2006) at line 3 yielded a value of 30°. As expected, the airstrip also has a very steep cliff slope, with a value of 41° (line 5, 2006-2012). Cliff slope values do not correlate with mean erosion rates (correlation coefficient of 0.05, no statistical significance).

In summary, at the Komakuk site no shore profile component shows a significant correlation with mean annual erosion rates. To assess whether the combination of the factors which are strongest correlated with the mean annual erosion rate can better explain the variability of coastal erosion a multiple regression analysis was performed. The r^2 value for the parameters beach width and absolute cliff height equals to 0.13.

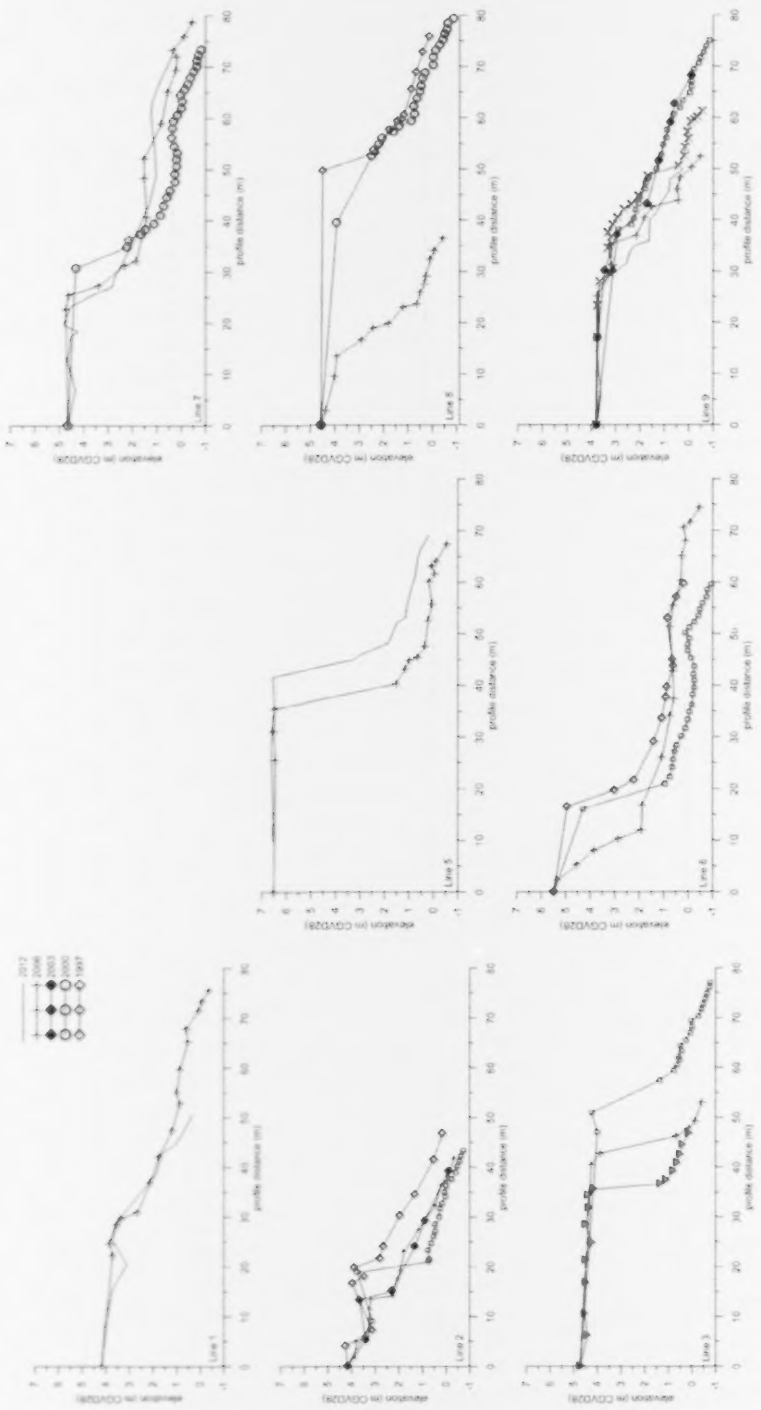

Figure 14: Shore profiles for the Komakuk site generated from GPS measurements. CGVD28 is the Canadian Geodetic Vertical Datum 1928. For transect position see Figure 8.

Table 13: Mean shoreface profile statistics for the Komakuk site and correlation of each factor with erosion rates. ER is the erosion rate, r is the correlation coefficient.

Line no.	Time period	Beach width [m]	Beach slope [deg]	Rel. cliff height [m]	Abs. cliff height [m]	Cliff slope [deg]	Mean ER [m/a]
1	2006-2012	27.60	5	1.52	3.79	9	-1.00
2	2000-2003	16.60	4	2.19	3.70	45	-1.84
	2003-2006	23.15	5	1.14	3.42	45	-0.52
3	2000-2006	3.70	12	3.62	4.06	30	-0.72
	2006-2012	4.38	12	3.42	4.02	48	-1.20
5	2006-2012	21.87	4	4.81	6.51	41	-0.56
6	1997-2000	20.66	3	2.48	3.65	22	-0.16
	2000-2006	33.37	3	3.38	4.81	27	-1.37
7	2000-2006	24.88	1	3.16	4.59	15	-0.24
	2006-2012	32.94	2	3.42	4.47	18	-0.90
8	1997-2000	10.93	3	3.21	4.21	18	-0.57
	2000-2006	6.68	4	3.17	3.92	18	-0.96
9	2000-2003	12.08	4	2.09	2.92	6	-2.27
	2003-2006	12.13	2	2.50	3.07	12	-0.71
	2006-2012	9.21	3	2.42	3.44	16	-1.43
r		0.24	-0.04	0.23	0.34	0.05	/
Significant at α=0.05		No	No	No	No	No	/

DSAS analysis

Two ArcMap tables are generated from each DSAS calculation, one containing the intersection points in the form of spatial x and y coordinates, the other containing the shoreline statistics. The first section below presents the results obtained from the DSAS analyses of several shorelines at once. For the calculations for the entire coast (638 transects), the shorelines from 1951, 1972 and 2009 were used. The calculations for the Border site (48 transects) include the shorelines from 1951, 1972, 1994 and 2009. For the Komakuk site (21 transects), shorelines from the years 1951, 1964, 1975, 1984, 1992 and 2009 were analyzed. In the subsequent sections, the results are presented for the DSAS analysis of two shorelines at

a time, thus providing information about shoreline changes between time periods. The results are reported to two decimal places but this does not necessarily indicate such a high accuracy.

DSAS results of complete time series

Table 14 shows a summary of all DSAS statistics calculated for the entire study area, for the Border site, and for the Komakuk site. A graph of the shoreline change envelope (SCE) which is the distance between the shorelines farthest from and closest to the baseline, and the net shoreline movement (NSM) which is the distance between the oldest and youngest shorelines provides an overview of the spatial variance in shoreline dynamics and the total shoreline change along the 35 km of investigated coast (Figure 15). The graph illustrates that the area between the border and Clarence Lagoon has some of the highest SCE and NSM values. The values decrease towards Clarence Lagoon, where they are lowest. Between Clarence Lagoon and Backhouse River the values steadily increase with a peak about 1 km east of Clarence Lagoon. East of the Backhouse River values decrease before they increase again in the block failure zone. East of the block failure area, coastal dynamics and coastal recession steadily decrease towards Komakuk. The highest cumulative erosion was calculated for transect number 443 at the end of a high cliff section just east of Clarence Lagoon, with a total retreat of 121.94 m (Figure 15), while the only accumulation was measured at the Clarence Lagoon spit, amounting to an advance of 11.39 m (transect 492). At the Border site, the highest of NSM was -114.03 m, whereas at Komakuk, the highest NSM was -68.67 m. The variation in mean NSM among the study areas is smaller, amounting to -72.67 m for the entire area, and to -78.94 m and -54.98 m for the Border and Komakuk sites, respectively. The SCE statistic gives some indication of overall shoreline dynamics, and was lowest for transect 479 at the eastern end of Clarence Lagoon, with a total shoreline movement of just 5.29 m. Just 1820 m to the east is the transect with the largest shoreline movement (transect 443, SCE of 121.94 m).

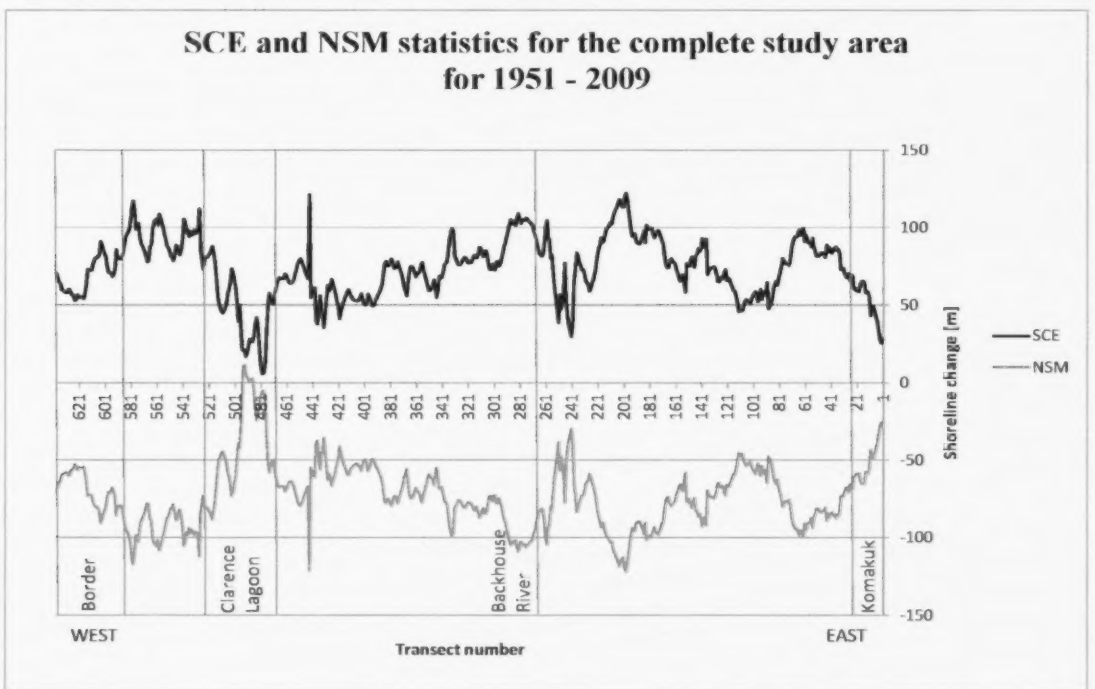

Figure 15: Shoreline change envelope (SCE) and net shoreline movement (NSM) statistics for the entire study area.

The end point rate (EPR), least median of squares (LMS), weighted linear regression rate (WLR) and linear regression rate (LRR) are all statistical measures of annual shoreline change. Despite the differences between the rates, some basic patterns of mean erosion can be distinguished for each study area. For the entire study area, the mean annual erosion varies between -1.24 ± 0.38 m/a (LRR), and -1.31 ± 0.39 m/a (WLR). The mean erosion values for the Border site are higher, with mean rates ranging from -1.20 ± 0.37 m/a (WLR) to -1.36 ± 0.25 m/a (EPR), whereas the Komakuk site has lower mean erosion rates, ranging from -0.62 ± 0.18 m/a (LMS) to -0.95 ± 0.16 m/a (EPR). These results explain why the SCE and NSM values are lower than average at Komakuk and higher than average for the Border site. Table 14 also displays the minimum and maximum values for each statistic, showing that large variations can occur on different transects. An evaluation of the DSAS results for all transects in the study area shows that, of the 638 transects, eight have positive annual rates of change, being highest at transect 492 with a value of 0.20 m/a (EPR). The highest annual shoreline erosion amounts to -2.20 m/a (transect 210, WLR).

The supplemental statistics for the EPR, WLR and LRR values give additional information about the robustness of the respective rates. The ECI value indicates the confidence of the EPR. The EPR values are more reliable the lower the ECI is. As the ECI is calculated from the uncertainties of the youngest and oldest shorelines, and the same oldest and youngest shorelines have been used for each analysis, the ECI has a consistent value of 0.18 m/a. The coefficients of determination for the LRR and WLR statistics (LR2 and WR2) indicate how much percent of the variation in the data is explained by the respective regression line. The means of both values are very high for each study site. Except for the Komakuk site with an LR2 value of 84%, all WR2 and LR2 values for each site are higher than 90%. Further supplemental statistics are the 95% confidence interval values (LCI95 and WCI95) which indicate the range in which one can be 95% confident that the true rate of change lies. The values are highest for the entire study area calculations (WCI95=3.34 m) and lowest for the Border site (WCI95= 0.31 m). Standard errors (LSE and WSE) show the average distance of the estimated to the actual value. They are higher for the linear regressions than for the weighted ones, with mean LSE values exceeding WSE values several fold.

Despite the fact that the LRR values have poorer supplemental statistics than the WLR values, the LRR values are assumed to be most reliable and were thus used as reference values for further analyses. Although the WLR values account for an assigned uncertainty in measurement, in some cases this can significantly influence the rate of change and consequently, inaccurate determination of the uncertainty results in less accurate determination of erosion rates. When calculating rates over multiple time periods, shoreline change rates calculated for the EPR are considered to be less reliable than LRR values, as the EPR method considers only the youngest and oldest shorelines and thus does not fully account for shoreline dynamics. In LMS calculations, the influence of outliers is weakened. Outliers can be the result of digitization mistakes, but they can also represent coastal response to an unusually calm or stormy period of time. Thus, the LMS calculations lead to a better determination of average coastal change rates under normal conditions, but on the other hand, they weaken the influence of extreme meteorological events, which are considered the most effective agents of coastal change.

Table 14: Summarized mean DSAS outputs for the entire study area, the Border and Komakuk sites. σ is the standard deviation. For explanations of statistical output abbreviations see Table 4.

		SCE [m]	NSM [m]	EPR [m/a]	ECI [m/a]	LMS [m/a]	WLR [m/a]	WSE [m/a]	WR2	WCI95 [m/a]	LRR [m/a]	LSE [m/a]	LR2	LCI95 [m/a]
Entire study area	Min	5.29	-121.94	-2.10	0.18	-2.13	-2.20	0.00	0.04	0.00	-2.17	0.00	0.00	0.00
	Max	121.94	11.39	0.20	0.18	0.19	-0.08	6.82	1.00	12.75	0.24	27.88	1.00	8.52
	Mean	**73.20**	**-72.67**	**-1.25**	0.18	**-1.25**	**-1.31**	**1.79**	**0.93**	**3.34**	**-1.24**	**7.30**	**0.95**	**2.23**
	σ		21.62	0.37		0.37	0.39				0.38			
Border site	Min	51.36	-114.03	-1.96	0.18	-1.96	-1.88	0.09	0.88	0.02	-1.93	0.54	0.92	0.05
	Max	114.03	-51.36	-0.88	0.18	-0.75	-0.58	2.48	1.00	0.68	-0.84	11.13	1.00	1.09
	Mean	**78.94**	**-78.94**	**-1.36**	0.18	**-1.31**	**-1.20**	**1.14**	**0.99**	**0.31**	**-1.33**	**5.20**	**0.98**	**0.51**
	σ		14.78	0.25		0.29	0.37				0.27			
Komakuk site	Min	33.92	-68.67	-1.18	0.18	-0.97	-1.28	1.81	0.71	0.12	-1.11	2.87	0.68	0.17
	Max	68.67	-33.92	-0.58	0.18	-0.36	-0.37	6.52	0.99	0.43	-0.58	14.08	0.96	0.84
	Mean	**54.98**	**-54.98**	**-0.95**	0.18	**-0.62**	**-0.79**	**4.34**	**0.91**	**0.29**	**-0.88**	**8.71**	**0.84**	**0.52**
	σ		9.48	0.16		0.18	0.25				0.15			

DSAS results for time period analysis for the entire study area

In contrast to the variety of methods available in DSAS for calculating erosion rates over multiple time periods, to develop a time series of erosion, an approach using single time steps is adopted. The EPR method is most appropriate for this type of analysis, since no regression analyses can be provided for only two shorelines.

Shoreline changes across the entire study area in the two time periods under investigation are shown in Table 15. Results show a deceleration of mean coastal erosion from -1.35 ± 0.55 m/a between 1951 and 1972, to -1.18 ± 0.52 m/a between 1972 and 2009, a difference of 13.39%. However, an evaluation of the individual transect results showed that, for 42% of the transects, there was an acceleration of erosion between the first and second periods, whereas the remaining 58% showed a deceleration or no change. The box-whisker plots shown in Figure 16 depict the spread of transect values for both time periods. In addition to erosion rates, the variability of erosion rates has changed through time (Figure 16). In the first time period, the data were distributed more uniformly, with the mean and median value lying very close to each other, and a low number of extreme values. In the second time period, although the mean erosion rate decreased, the variability of the lowest and highest quartiles increased, leading to a higher number of extreme values. However, variability in the central quartiles decreased in comparison to those of the first time period.

Map 1 (Appendix V) illustrates the EPR values for both time periods, thus showing the spatial distribution of shoreline dynamics. The area just west of Komakuk shows a deceleration in erosion, whereas the area of block failures further west reveals consistently high rates of coastal recession. An acceleration of coastal erosion can be seen around the two channels entering the Beaufort Sea just west of the Backhouse River. Comparatively low erosion rates are seen west of this along an approximately 8 km long stretch of coast which extends to the western end of Clarence Lagoon. The area between Clarence Lagoon and the Border site has comparatively high shoreline dynamics and shows increasing erosion rates.

Table 15: Mean shoreline change values for each time period for the entire study area. EPR stands for end point rate, NSM stands for net shoreline movement. Negative variation which shows a decrease in the erosion rate from the mean is indicated by ↓.

Time period	Measure	Mean EPR [m/a]	Mean NSM [m]	Variation to overall LRR [%]
1951-1972	Max	-0.06	-1.23	
	Min	-2.65	-55.69	
	Mean	-1.35 ± 0.55	-28.23	8.49
1972-2009	Max	0.76	28.13	
	Min	-2.85	-105.59	
	Mean	-1.18 ± 0.52	-43.69	↓4.90
Site LRR [m/a]		-1.24 ± 0.38		

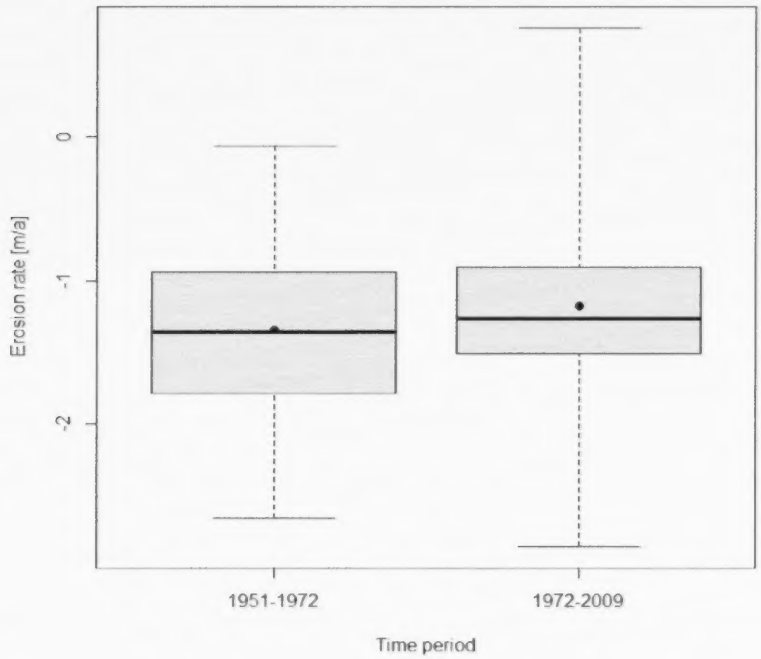

Figure 16: Box-whisker plots showing erosion rates for the entire study area. The box comprises the data range between the lower (Q1) and upper (Q3) quartile, the median (Q2) is indicated by the line, the mean by the point. The whiskers indicate the smallest and largest value.

DSAS results for time period analysis for the Border site

At the Border site, DSAS results show that erosion rates are highest for the two short periods from 1972 to 1976 and from 1992 to 1994, with values of -1.94 + 1.12 m/a and -1.99 + 1.16 m/a, respectively (Table 16). Moreover, these rates have very high standard deviations of up to 58%. However, these rates were not taken into account for the calculation of the overall shoreline dynamics presented in subsection 4.2.1 in order to calculate the statistics using time steps of comparable lengths. The EPR values for the three main time periods show that between the first and second time period erosion decelerated, from -1.28 ± 0.41 m/a to -1.15 ± 0.40 m/a. This deceleration is followed by an acceleration in mean erosion over the last time period, with the mean erosion rate increasing to -1.79 ± 0.35 m/a. This high variation is also clearly visible in Figure 17. The difference in the erosion rate distributions in the second and third time periods is very high, with the middle 50% of the values for the second time period spanning the same range as the lowest 25% of all values for the third time period. As was the case with the box-whisker plots for the entire study area, the range of outliers at the Border site is greatest for the last measured time period.

Map 2 (Appendix VI) displays the EPR results for the three time periods used at the Border site. Whereas the eastern part of the Border site shows high erosion rates for all time periods, in the western part of the study area, erosion rates were low in the first time period and accelerated thereafter. Thus, the study area has highly variable shoreline erosion dynamics occurring in close proximity.

Table 16: Mean shoreline change values for each time period for the Border site. EPR stands for end point rate, NSM stands for net shoreline movement. Negative variation which shows a decrease in the erosion rate from the mean is indicated by ↓.

Time period	Measure	Mean EPR [m/a]	Mean NSM [m]	Variation based on site LRR [%]
1951-1972	Min	-2.15	-45.06	
	Max	-0.67	-14.00	
	Mean	-1.28 ± 0.41	-26.82	3.69
1972-1976	Min	-4.35	-17.39	
	Max	-0.08	-0.33	
	Mean	-1.94 ± 1.12	-7.74	↓45.92
1972-1994	Min	-0.21	-4.72	
	Max	-1.88	-41.30	
	Mean	-1.15 ± 0.40	-25.24	13.63
1992-1994	Min	-4.70	-9.08	
	Max	-0.13	-0.26	
	Mean	-1.99 ± 1.16	-3.85	↓50.17
1994-2009	Min	-2.61	-39.19	
	Max	-0.97	-14.54	
	Mean	-1.79 ± 0.35	-26.88	↓34.63
Site LRR [m/a]		-1.33 ± 0.27		

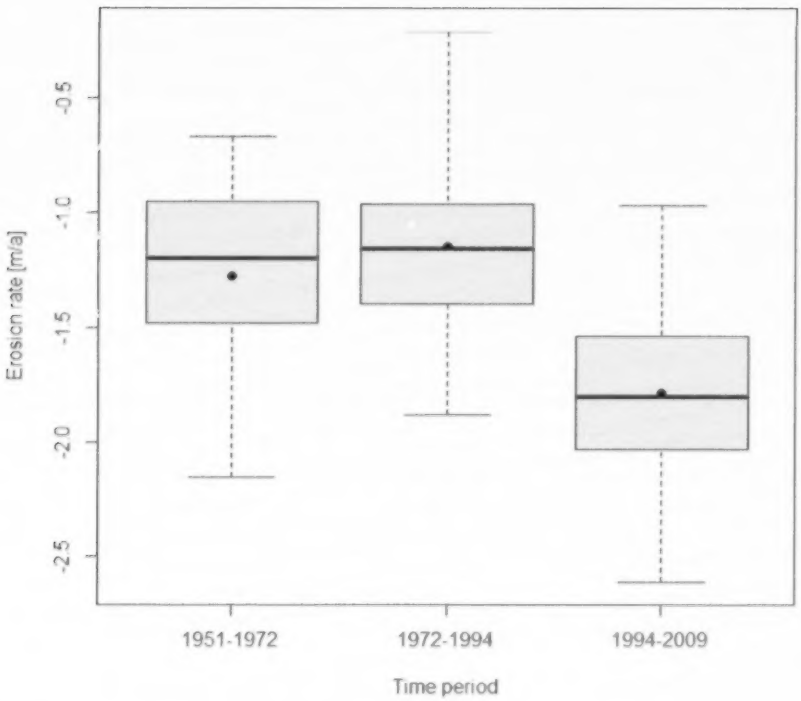

Figure 17: Box-whisker plots showing erosion rates for the three main time periods used for the Border site. The box comprises the data range between the lower (Q1) and upper (Q3) quartile, the median (Q2) is indicated by the line, the mean by the point. The whiskers indicate the smallest and largest value.

DSAS results for time period analysis for the Komakuk site

In contrast to the Border site, single time period analysis results for the Komakuk site reveal a clear and steady trend towards a comparatively rapid deceleration of mean annual erosion rates. Highest rates of coastal erosion were calculated for the first time period between 1951 and 1964 with a mean of -1.92 ± 0.62 m/a. The EPR values steadily decrease with every time step and are lowest for the time period between 1992 to 2009, with a mean annual erosion of -0.49 + 0.27 m/a. Results for two shorter time periods from 1972 to 1975 and 1992 to 1993 also suggest decelerating erosion. Figure 18 shows that both the range of the middle 50% of rates, as well as the range of the outliers narrows with time. However, erosion rates which are more negative than the median are more widely scattered than erosion rates which are closer to zero. This distribution pattern lowers the mean erosion rate for each time period.

Map 3 (Appendix VII) depicts the temporal and spatial distribution of the EPR values. The area east of the airstrip has low erosion rates for all time periods. The area around the airstrip shows a deceleration of erosion beginning in the 1970's. The highest shoreline dynamics occur in the western section of the Komakuk site, with a deceleration of annual coastal erosion from more than -2.00 m/a to less than -0.50 m/a.

In summary, the overall trend of the entire study sites shows decreasing mean annual erosion rates. This trend is confirmed by decadal calculations of shoreline change for the Komakuk site, whereas the local mean annual erosion rates are lower. DSAS analyses of the Border site differ from the overall trend of decreasing erosion rates, as results from the last time period show a renewed acceleration in erosion.

However, GPS analyses from the Border site are contradicting the DSAS results as they show constantly decreasing erosion rates since 1991.

Table 17: Mean shoreline change values for each time period for the Komakuk site. EPR stands for end point rate, NSM stands for net shoreline movement. Negative variation which shows a decrease in the erosion rate from the mean is indicated by ↓.

Time period	Measure	Mean EPR [m/a]	Mean NSM [m]	Variation based on site LRR [%]
1951-1964	Min	-1.38	-40.88	
	Max	-0.75	-9.71	
	Mean	-1.92 ± 0.62	-24.99	↓119.25
1964-1972	Min	-1.38	-24.62	
	Max	-0.49	-3.94	
	Mean	-1.53 ± 0.72	-12.18	↓74.71
1972-1984	Min	-2.21	-6.56	
	Max	-0.20	-0.60	
	Mean	-1.16 ± 0.55	-3.45	↓32.46
1972-1975	Min	-1.38	-6.56	
	Max	-0.20	-0.60	
	Mean	-1.16 ± 0.55	-3.45	↓32.46
1984-1992	Min	-1.38	-13.38	
	Max	-0.01	-0.08	
	Mean	-0.53 ± 0.42	-4.22	39.48
1992-1993	Min	-1.38	-29.41	
	Max	0.35	3.21	
	Mean	-0.95 ± 0.43	-8.41	↓8.48
1992-2009	Min	-1.01	-17.17	
	Max	-0.08	-1.33	
	Mean	-0.49 ± 0.27	-8.36	43.72
Site LRR [m/a]		-0.86 ± 0.15		

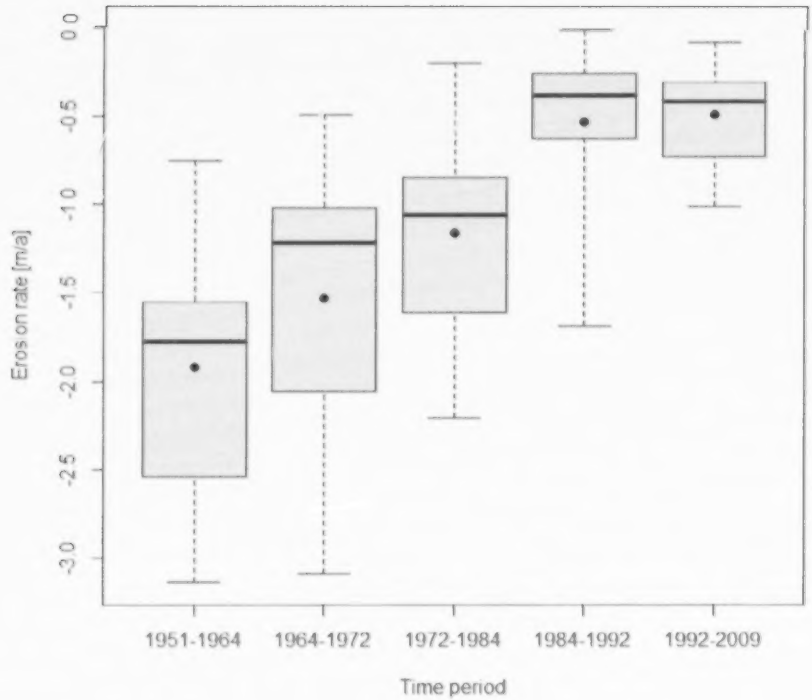

Figure 18: Box-whisker plots showing erosion rates for the five main time periods used for the Komakuk site. The box comprises the data range between the lower (Q1) and upper (Q3) quartile, the median (Q2) is indicated by the line, the mean by the point. The whiskers indicate the smallest and largest value.

Calculation of total land loss

Based on differences in the shoreline position and estimated cliff heights, the total area and volume of land loss between 1951 and 2009 was calculated for the entire study site. The calculations yield a total land loss 2,607,600 m², which amounts to approximately 4.5 ha/a. The total eroded volume was calculated to be 14,301,207 m³, amounting to approximately 250,000 m³ per year.

Discussion

Three areas of research introduced in previous chapters bear further discussion. These are: the variability of erosion rates for each study site; the strengths and weaknesses of the DSAS and GPS methods; and the correlations of shore profile parameters with mean erosion rates.

Variability of erosion

Entire study area

Results from the DSAS analyses spanning the 58 year record of historical aerial photography show a decelerating trend in mean annual erosion, as well as temporal and spatial variability of mean annual erosion rates in the study area. For example, the area of block failures to the west of Komakuk is particularly striking in terms of consistently high erosion rates. This might be attributable to the fact that, in this area, the beach is very narrow or even missing, so that the cliff is constantly subject to wave action.

Since the cliff is not very high and contains large amounts of ground ice, the waves are able to rapidly remove any eroded material, so that no protective beach forms. However, this coastal process is locally restricted, as the block failure area is bordered by areas which show decreasing erosion rates. On the other hand, most areas in which cliff morphology is primarily a function of thermal denudation processes appear to have stabilized over time and show a deceleration of erosion. Nevertheless, such cliffs are known to show periodic reactivation, so renewed acceleration of coastal erosion in these areas is not unlikely (Lantuit et al. 2008).

The overall trend of decreasing mean erosion was also reported for the study area in reports of ground survey studies conducted by McDonald and Lewis (1973), Forbes and Frobel (1985), Forbes et al. (1995), Solomon (1998) and Lantuit and Pollard (2008). However, these results are in contrast to findings by Covill (1997) for the western Yukon, and to several studies for the Alaskan part of the Beaufort Sea coast (Brown et al. 2003; Jones et al. 2009; Ping et al. 2011) which show a trend towards accelerating coastal retreat and generally higher mean erosion rates (Table 1).

Border site

At the Border site, a slightly different coastal change pattern was determined from the DSAS results. During the earliest time period of the analysis, from 1951 to 1994, results followed the overall trend of the entire study area and show a deceleration of erosion, followed by an acceleration of erosion during the later time period from 1994 to 2009. The recent acceleration trend seen in the DSAS results is in accordance with findings from nearby on the Alaskan Beaufort coast. Ping et al. (2011) also calculated an acceleration of coastal erosion since the mid-1990's using satellite images and aerial photography between the border and Demarcation Point. Further to the west, in the Teshekpuk Lake area, the same tendency was observed by Mars & Houseknecht (2007) who used topographic maps and Landsat thematic mapper data, and by Jones et al. (2009) who conducted DSAS analyses on the basis of aerial photography. However, despite the fact that these studies show the same tendency in mean annual erosion as the DSAS results, they should not be used to conclusively verify the DSAS findings from the Border site because of differences in methodology and study area morphology. For example, the results obtained by Ping et al. (2011) show significantly higher erosion rates with a mean rate of -3.88 m/a for the time period between 1980 and 2000. This high rate may be attributable to the fact that Ping et al. (2011) determined rates of change on the basis of a DSAS analysis of a 1 km long study area and extrapolated this value to the whole region. The DSAS results of the research presented here show that alongshore rates of shoreline erosion are highly variable, suggesting that results from a 1 km length of coast may not represent the rate of shoreline erosion of a larger study area, unless the coastline is homogeneous. The studies of Mars and Houseknecht (2007) and of Jones at al. (2009) both focus on a region which has a different shoreline morphology than the Border site, as it is comprised of breached thermokarst lakes. Thus it can be expected to show different erosion rates than the Border site, and the shoreline change dynamics may not be comparable.

In contrast to the acceleration in erosion given by the DSAS results between 1994 and 2009, the GPS analyses from 1991 to 2012 encompass a similar time span, but show no significant changes in erosion rates. Since the GPS results have a higher spatial resolution, they are likely more trustworthy.

Other studies provide additional information about long-term trends in erosion rates at the Border site. When the monument was established at the international border in 1912, the distance to the cliff was measured. McDonald and Lewis (1973) calculated an erosion rate for the time period between 1912 and 1972 of -0.72 m/a. Results of a second survey by Forbes and Frobel (1985) in 1984 give a mean annual erosion rate from 1972 to 1984 of -0.83 m/a. These two rates extend the late 20th century surveys back to 1912 and show that, at the Border site, mean annual erosion rates increased from the early 20th century until the early 1990's, peaked, and then decreased.

The changing long-term trends may be explained to some extent by meteorological conditions. Annual wind speeds and the frequency of storms coming from the north-west are considered to be most effective in causing shoreline change (Solomon et al. 1994; Manson & Solomon 2007). According to Manson and Solomon (2007), two periods of increased wind speeds occurred between 1960 and 1966 and between 1986 and 1995, and a period of lower wind speeds occurred between 1995 and 2000. The stormy period from the mid-1980's to the mid-1990's may be the reason for the high DSAS erosion rate (-1.99 ± 1.16

m/a) seen in the 1992 to 1994 time period. Coastal change rates measured over short time periods are known to be prone to variability of environmental forcing, which can be especially large in high latitude environments (Dolan et al. 1991; Dallimore et al. 1996; Solomon 2005). At Tuktoyaktuk, for example, observed coastal erosion from single storm events highly exceeded long term mean annual erosion rates (Solomon et al. 1994, after Aveco 1986).

Komakuk site

DSAS results from the Komakuk site show steadily decreasing erosion, so the site specific values match well with the overall trend for the entire study site. These results are in accordance with the tendencies found in other studies conducted at Komakuk by Forbes et al. (1995) and Solomon (1998), although the rates calculated in this study are slightly lower than those of Solomon (1998), and slightly higher than those of Forbes et al. (1995). The GPS analyses provide a higher temporal resolution of shoreline change for the last 15 years and show the same tendency as the DSAS results. Since the Komakuk site includes the gravel airstrip, local small scale spatial differences in erosion rates can be seen. The comparatively lower erosion rates of the gravel airstrip in comparison to the adjacent fine-grained ice-rich cliff suggest that grain sizes influence erosion rates. This is reasonable since more wave energy is needed for the transport of coarser grain sizes. The importance of grain size for the local coastal erosion pattern was also emphasized by Reimnitz et al. (1985, 1988).

In summary, a comparison of all three study areas leads to the recognition of a spatial pattern in coastal erosion, since at the very east of the study region, the Komakuk site shows low and decelerating erosion rates, whereas at the very west of the study region, the Border site shows higher and accelerating erosion rates. The mean erosion rate for the entire study area lies in between the rates of both sites. By including studies from the Alaskan part of the Beaufort Sea, this spatial pattern of accelerating mean erosion can be extended even further west (Mars & Houseknecht 2007; Jones et al. 2009; Gibbs et al. 2011).

Evaluation of methodology

The processing of imagery used in the DSAS investigations is important for assessing the accuracy of the results. The foundation of the DSAS analysis is provided by remote sensing data (i.e. aerial photography and satellite images) on which the shorelines are digitized. For this study, the photos were scanned with a sub-metre pixel resolution and georeferenced/co-registered with a mean RMS error of 1.3 m (minimum: 0.47 m, maximum: 2.63 m). Considering the scarcity of clearly distinguishable reference points in most of the study area, these RMS errors are fairly good and compare well to other studies (Brown et al. 2003; Solomon 2005; Jones et al. 2008). The most recent shoreline used in the analyses is from 2009 and was digitized from a SPOT image with a ground resolution of 10 m.

Given that the aerial photography was scanned to give a resolution of approximately 1 m, the 10 m resolution SPOT imagery presents challenges for the interpretation and digitizing of shorelines. Thus the single time period DSAS calculations for the Border and Komakuk site which use the 2009 shoreline might be potentially less accurate than the other time periods. By examining individual DSAS and GPS transects for the Border and Komakuk sites from each method, a general sense of the accuracy of the DSAS results was obtained. Individual DSAS transects were selected which were located the closest to the GPS transects at each study site, and the erosion rates were compared for the most recent time period available for each method. At the Border site, three transects were examined, with the DSAS transects covering the period from 1994 to 2009, and the GPS ones the period from 1991-2012. The mean difference in erosion rates between the two methods at the Border site was 0.46 m/a. At the Komakuk site, a total of three transects was also examined; the DSAS transects covered the period from 1992 to 2009, and the GPS covered the time period from 2000 to 2012. The mean difference in erosion rates between the two methods at the Komakuk site was 0.10 m/a. So although a common data base for a complete and direct comparison of the two methods is missing, the data that are available enable the highly accurate GPS results to legitimize the results obtained from the DSAS analyses.

The two regression rates calculated by DSAS, the linear regression rate (LRR) and the weighted linear regression rate (WLR), help in determining the robustness of the calculated erosion rates, but a comparison of the two regression rates can also help in interpreting how important the shoreline

uncertainty of the SPOT image might be. The long-term mean erosion rate calculated by DSAS for the entire study area using the LRR method is -1.24 m/a. In contrast, The WLR value calculated by DSAS indicates faster annual erosion with a mean of -1.31 m/a. It is not surprising that the LRR and WLR values differ, since only three different time periods were considered for the entire coast (1951, 1972, 2009) and the most recent calculation uses the 2009 SPOT shoreline. Since the most recent time period has lower erosion rates and the 2009 shoreline is weighted less due to its uncertainty, the overall WLR value is higher. The total difference between the LRR and the WLR is nevertheless still very small, amounting to 0.07 m. The differences between the LRR and the WLR at the Border and Komakuk sites are comparable, with values of 0.13 m and 0.09 m, respectively. Extrapolating these differences to the entire time period of measurements (58 years) results in NSM differences of less than 10%, so they are thus considered to be negligible. However, this example shows that it is important to be aware of the quality of each data set in order to be able to interpret the overall quality of the DSAS findings. Overall, both the LRR and the WLR rate coincide well with the mean annual coastal change rate for the entire Canadian Beaufort coast of -1.12 m/a, taken from the Arctic Coastal Dynamics database (Lantuit et al. 2011).

A constraint which applies to both the DSAS and the GPS methods is the spacing of the measurements, since the possibility always exists that the analyzed points do not adequately capture the prevailing shoreline dynamics. This problem can be countered, but not fully prevented, by a finer transect spacing. However, too fine spacing can unnecessarily increase the amount of output data without improving the quality of the outcomes. The GPS transects provide valuable information about spatial changes of the shore profile morphology and could thus be used in future analyses to help determine if the 50 m DSAS transect spacing is adequate.

In summary, the GPS measurements provide valuable reference data which help to validate the quality of the DSAS results, even if differences in study area exist, transect positions and time periods complicate a direct one-to-one comparison of both values. Against the backdrop of published shoreline change studies, the DSAS results are believed to accurately indicate the overall trend of decelerating coastal erosion along most of the western Yukon coast and accelerating coastal change near the border, even though the quality of the results may not be considered sufficient for the determination of coastal change rates with sub-metre accuracy. The incorporation of recently acquired very high resolution satellite imagery into the DSAS analyses may help constrain the present erosion rates.

Correlations of shore profile parameters with erosion

One goal of this study was to explore whether shore profile parameters can help explain variability in coastal dynamics. The results from the GPS surveys show that the shore profile statistics from both the Border and Komakuk study sites vary greatly and that, except for the relative cliff height, all shore profile parameters are more distinctly correlated with mean annual erosion rates at the Border site. Simple regression analyses for the Border site show a very strong and statistically significant correlation between beach widths and mean annual erosion rates ($r=0.84$), and a strong but statistically insignificant correlation between absolute cliff heights and mean annual erosion rates ($r=0.70$). At the Komakuk site, no correlation with mean annual erosion and no significance of any variable was found. However, the highest correlations were also distinguished for absolute cliff heights ($r=0.34$) and for beach widths ($r=0.24$).

The large variations between the correlation coefficients at the two sites can be partly explained by different site morphology. The Border site is a short and homogeneous stretch of coast. Shore profile statistics and mean annual erosion rates both show low variability. The homogeneity of the data means that the relation between the independent and dependent variable of each data pair (e.g. beach width value and its respective erosion rate) varies less. This leads to a lower deviation of the data pairs from the regression line, so that the variability in the data is better explained by the regression model, suggesting the data is more highly correlated. In contrast, the Komakuk site has a more heterogeneous shoreline morphology. Shore profile statistics and mean annual erosion rates both show high variability. In order to assess how well shore profile parameters in general explain variations in mean annual erosion along the western Yukon coast, this site serves as a better reference, since it includes different shore profile morphologies. Thus, even though the correlation coefficients calculated for the Komakuk site are lower,

they are considered to be more meaningful in terms of the overall mean correlation of beach widths and erosion rates. In addition, the calculations for Komakuk are also more robust because they were conducted with a higher number of data pairs (N=15) than at the Border site (N=7). At the Border site, the statistically significant very strong positive correlation of beach widths with the respective mean erosion rates suggests that erosion is mainly governed by beach widths, thus meaning the wider the beach is, the lower erosion is. In general, a correlation of these two factors is reasonable since the widening of the beach lengthens the distance which needs to be overtopped by the sea in order to reach the cliff face (Reimnitz et al. 1985). However, it is questionable if beach width actually does govern coastal erosion, even though the findings from the Border site suggest this conclusion. A factor which could have mistakenly led to such a high correlation is the small number of data pairs (N=7), as mentioned earlier. The correlation does have a statistical significance of 95%, meaning that there is only a 5% chance that the data are random. If the numbers are indeed correct, this would mean that beach width explains 71% (coefficient of determination between beach widths and mean erosion rates) of the measured variation in erosion, leaving 29% to be explained by other factors.

In general, the correlation of absolute cliff heights with mean annual erosion rates might be explained by the fact that after erosion occurs, more erosional debris has to be removed from the toe of the cliff before the cliff face is again exposed to further erosion. In contrast to the correlation coefficient of absolute cliff heights at the Border site, a similar statistic calculated by Héquette and Barnes (1990) shows a weak correlation of cliff heights with mean annual erosion rates ($r=0.29$). Moreover, they determined that erosion rates are only smaller for very high cliffs (> 20 m), thus implying that the amount of debris contributed by lower cliffs is not high enough to affect erosion (Héquette & Barnes, 1990; Lantuit et al. 2011). Héquette and Barnes calculated the correlation coefficient by using 16 data pairs from across the Canadian Beaufort coast and thus compiled a database which includes a number of different shore profile morphologies. A comparison of findings from the Komakuk site to the correlation coefficient from Héquette and Barnes indicates fairly good agreement, although the correlation coefficient of absolute cliff heights at the Komakuk site is slightly higher. Neither correlation coefficient is statistically significant indicating that although there is compelling evidence that cliff height and erosion rate are correlated, the data is insufficient to prove that.

In summary, the shore profile parameters explain variation in erosion to different extents at the Komakuk and the Border sites. While at least beach widths seem to influence coastal erosion at the Border site, at the Komakuk site, no shore profile parameter was found to adequately explain variability of shoreline retreat. However, it has to be remembered that the amount of data underlying the analyses was very small, which limits the credibility of the findings. A higher number of samples can raise the resistance of correlation coefficients to outliers and leads to a higher validity of the results.

The present findings lead to the conclusion that the importance of shore profile parameters in terms of guiding coastal erosion is relative and highly variable. However, given the fact that the Border site and the Komakuk site show similar patterns of coastal retreat, it could be assumed that erosion at both study sites may be governed by external factors which operate on a regional scale (i.e. environmental forcing). Solomon (1994), for instance, found strong correlation between coastal retreat and storm intensity. Kobayashi et al. (1999) modeled cliff response to storm surges and concluded that storm surge elevation and duration, seawater temperature and salinity, cliff height and frozen sediment characteristics are all important, as each factor influences certain parts of the erosion process. Lantuit et al. (2008) determined the correlation between erosion rates and ground ice contents and found a moderate but statistically significant correlation. Dallimore et al. (1996) also found that the form and volume of ground ice influences cliff response to coastal erosion. However, Aré et al. (2008) and Héquette and Barnes (1990) conclude that coastal erosion may be determined by ice in the water column rather than ice in the shore sediments, and that sediment transport by frazil ice and the process of ice gouging play major roles in determining coastal erosion.

In summary, the high spatial and temporal variability in coastal change which was distinguished along the western Yukon coast together with the locally very variable correlation of shore profile parameters with mean erosion suggest that, especially in such a cold climate environment, a wide range of factors contributes to coastal dynamics. It seems like their significance cannot be determined in an unambiguous way, but has to be defined in consideration of the specific site and conditions. Given that with continuing

climate change, environmental forcings such as the frequency of severe storms and overall wave energy are likely to increase as suggested by Manson and Solomon (2007), coastal retreat is expected to accelerate in the future.

Conclusions

The primary goal was to quantify coastal change along the western Yukon coast and, thus to give an overview of coastal dynamics in a high latitude environment through investigation of the spatial and temporal variability in cliff erosion rates. The contribution of geomorphologic variables (i.e. beach slope, beach width, cliff slope, absolute cliff height, relative cliff height) towards explaining changes in erosion rates was also considered in order to better understand processes governing Arctic coastal change.
According to the findings of the study, the following conclusions can be drawn:

- Mean annual erosion along the western Yukon coast is -1.2 m. The overall trend for the entire coast since the 1950`s is one of decreasing erosion, with rates declining from -1.4 m/a to -1.2 m/a, whereas this trend is nevertheless not statistically significant.
- Mean annual erosion at the Border site is -1.3 m/a based on the aerial photograph record, and -1.1 m/a based on survey measurements. The trend from aerial photographs shows no significant change except for an increase in erosion rates in the last two decades. Survey measurements show a decrease over this same 20-year period, but it is not statistically significant.
- Mean annual erosion at the Komakuk site is -0.9 m/a based on the aerial photograph record, and -1.1 m/a based on survey measurements. The trend from aerial photographs shows a steady and statistically significant decrease in erosion rates, with a slight but insignificant increase over the last two decades. Survey measurements show a decrease over a 15-year period, but it is not statistically significant.
- When compared to previous research in Alaska, the results from this work indicate a general spatial pattern in trends of erosion rates. Rates in Alaska are increasing, at the Border site have a slight increasing trend, and at the Komakuk site show a decreasing trend. Further studies might focus on explaining the reasons for such a pattern.
- Analyses of geomorphic parameters showed that beach width is significantly correlated with erosion rate at the Border site, but not at the Komakuk site. There is a strong but insignificant correlation with absolute cliff height at the Border site but again, not at Komakuk.
- Multiple regression shows that at the Border site, geomorphologic parameters explain 72% of the variability in erosion rates, whereas at Komakuk only 13% is explained. At both sites, the remainder likely relates to environmental forcing and ground ice contents. The difference between sites indicates that the response to potentially similar forcing can differ between various stretches of coast.
- Based on the calculated erosion rates, a mean area of 4.5 ha/a was lost between 1951 and 2009. The total volume of eroded material is 250,000 m^3/a. The measure of volumetric land loss presented here is a valuable contribution towards quantification of material fluxes for the region.

This work has provided information on temporal and spatial trends in cliff erosion for a highly dynamic region of the Canadian Beaufort Sea coast. An assessment of the geomorphological parameters shows to what degree they influence coastal erosion. Further work in the region could concentrate on assessing the influence of other parameters and would further deepen our understanding of the forces driving coastal change.

Acknowledgements

This research was conducted as part of the lead author`s master thesis at the Christian-Albrechts Universität zu Kiel, Germany. Funding provided by the German Academic Exchange Service in form of a scholarship for abroad research and by the Arctic Coastal Infrastructure Project in the Climate Change Geoscience Program of the Earth Science Sector of Natural Resources Canada is gratefully

acknowledged. We wish to thank Donald Forbes and Dustin Whalen for scientific guidance and assistance in the field. The thoughtful review of Dustin Whalen is greatly appreciated.

References

AMAP (Arctic Monitoring and Assessment Programme) (2012). Arctic Climate Issues (2011). Changes in arctic snow, water, ice and permafrost. SWIPA 2011 Overview Report.

Anisimov, O.A., Vaughan, D.G., Callaghan, T.V., Furgal, C., Marchant H., Prowse, T.D., Vilhjálmsson, H. & Walsk, J.E. (2007). Polar regions (Arctic and Antarctic) (653-685) *in* Parry, M.L., Canziani, O.F., Palutikof, J.P., van der Linden, P.J. & Hanson, C.E. (Eds.): Climate Change 2007: Impacts, adaptation and vulnerability. Contribution of Working Group II to the Fourth Assessment Report of the Intergovernmental Panel on Climate Change. Cambridge, UK, New York, USA.

Aré, F., Reimnitz, E., Grigoriev, M., Hubberten, H.-W., & Rachold, V. (2008). The influence of cryogenic processes on the erosional arctic shoreface. Journal of Coastal Research, 241, 110–121.

Aré, F. (1988). Thermal abrasion of sea coasts. Polar Geography and Geology, 12, 1–157.

Arens, T., Hettlich, F., Karpfinger, Ch., Kockelkorn, U., Lichtenegger, K. & Stachel, H. (2010). Mathematik (p. 1512). 2nd edition. Heidelberg. Germany.

Atkinson, D. (2005). Observed storminess patterns and trends in the circum-Arctic coastal regime. Geo-Marine Letters, 25(2-3), 98–109.

Bird, E. (2009). Coastal geomorphology – an introduction (p. 434). 2nd edition. Chichester, UK.

Boak, E. H., & Turner, I. L. (2005). Shoreline definition and detection: a review. Journal of Coastal Research, 214, 688–703.

Brown, J., Jorgenson, M., Smith, O., & Lee, W. (2003). Long-term rates of coastal erosion and carbon input, Elson Lagoon, Barrow, Alaska. Eighth International Conference on Permafrost (pp. 21–25).

Brown, J., & Solomon, S.M. (1999). Arctic Coastal Dynamics - report of an international workshop. Geological Survey of Canada Open File Report 3929 (p. 31).

Brown, R.J.E., & Kupsch, W.O. (1974). Permafrost terminology. National Research Council of Canada. (p. 62).

Bruun, P. (1954). Coast erosion and the development of beach profiles. Beach erosion board technical memorandum. No. 44. U.S. Army Engineer Waterways Experiment Station. Vicksburg, MS.

CCOG (Canadian Council of Geomatics) (2013) GeoBase Orthoimage 2005-2010. <http://www.geobase.ca/geobase/en/data/imagery/imr/description.html> (accessed: 06. Mar 2013).

Couture, N.J. (2010). Fluxes of soil organic carbon from eroding permafrost coasts, Canadian Beaufort Sea. Unpublished PhD thesis, McGill University, Montreal. (pp.136).

Couture, N J., Hoque, Md. A. & Pollard, W.H. (2008). Modeling the erosion of ice-rich deposits along the Yukon Coastal Plain. Conference Proceedings to the Ninth International Conference of Permafrost. University of Alaska Fairbanks.

Couture, N J., & Pollard, W.H. (2007). Modelling geomorphic response to climatic change. Climatic Change, 85(3-4), 407–431.

Covill, R. (1997). Photogrammetric analysis of coastal erosion at five sites in Ivvavik National Park, Appendix 1 *in* Forbes, D. L. 1997: Coastal erosion and nearshore profile variability in the southern Beaufort Sea, Ivvavik National Park, Yukon Territory. Geological Survey of Canada Open File Report no. 3531.

Dallimore, S.R., Wolfe, S., & Solomon, S.M. (1996). Influence of ground ice and permafrost on coastal evolution, Richards Island, Beaufort Sea coast, N.W.T. Canadian Journal of Earth Sciences, 33(5), 664–675.

Dolan, R., Fenster, M., & Holme, S. (1991). Temporal analysis of shoreline recession and accretion. Journal of Coastal Research, 7(3), 723–744.

Dupeyrat, L., Costard, F., Randriamazaoro, R., Gailhardis, E., Gautier, E., & Fedorov, A. (2011). Effects of ice content on the thermal erosion of permafrost: Implications for coastal and fluvial erosion. Permafrost and Periglacial Processes, 22(2), 179–187.

Eid, B.M., & Cardone, V.J. (1992). Beauford Sea extreme wave study. Environmental Studies Research Funds, Calgary; report series no. 114. (p. 143).

Forbes, D.L. (ed.) (2011). State of the Arctic Coast 2010 – Scientific review and outlook.IASC, LOICZ, AMAP, IPA. (p. 178) Geesthacht, Germany.

Forbes, D.L. (1997). Coastal erosion and nearshore variability in the southern Beaufort Sea, Ivvavik National Park, Yukon Territory. Geological Survey of Canada Open File report 3531. (p. 28).

Forbes, D.L. & Frobel, D. (1985). Coastal erosion and sedimentation in the Canadian Beaufort Sea. Current Research Part B, Geological Survey of Canada, Paper 85-1B. (p. 60-80).

Forbes, D.L., Solomon, S.M., & Frobel, D. (1995). Report of the 1992 coastal surveys in the Beaufort Sea. Geological Survey of Canada Open File 3053 (p. 39).

Forbes, D.L., & Taylor, R.B. (1994). Ice in the shore zone and the geomorphology of cold coasts. Progress in Physical Geography, 18(1), 59–89.

French, H.M. (2007). Periglacial Environment (p. 480). 3rd edition. The University of Ottawa, Canada.

Fritz, M., Wetterich, S., Schirrmeister, L., Meyer, H., Lantuit, H., Preusser, F., & Pollard, W.H. (2012). Eastern Beringia and beyond: Late Wisconsinan and Holocene landscape dynamics along the Yukon Coastal Plain, Canada. Palaeogeography, Palaeoclimatology, Palaeoecology, 319-320, 28–45.

GeoBase Canada (2012). Administrative boundaries. <http://www.geobase.ca/geobase/en/data/admin/index.html> (accessed: 19. Feb 2013).

GeoDZ (Geo Data Zone) (2010). Echtzeitkinematik. <http://www.geodz.com/deu/d/Echtzeitkinematik> (accessed: 19. Feb 2013).

Gibbs A., Harden E.L., Richmond, B.M. & Erikson L.H. (2011). Regional shoreline change and coastal erosion hazards in Arctic Alaska. Proceedings of the 2011 solutions to coastal disasters conference 2011, Anchorage, Alaska. (pp. 258-272).

Harper, J. (1990). Morphology of the Canadian Beaufort Sea coast. Marine Geology, 91, 75–91.

Harper, J.R., Reimer, P.D., & Collins, A.D. (1985). Beaufort Sea physical shore-zone analysis. Geological Survey of Canada Open File Report 1689. (p. 105).

Harris, S.A., French, H.M., Heginbottom, J.A., Johnston, G.H., Ladanyi, B., Sego, D.C., & Van Everdingen, R.O. (1988). Glossary of permafrost and related ground-ice terms. National Research Council of Canada. (p. 156).

Harry, D.G. (1988). Ground ice and permafrost *in* Clark, M. J. (ed.): Advances in periglacial geomorphology (p. 481). Chichester, UK.

Héquette, A., Ruz, M.-H., & Hill, P.R. (1995). The effects of the Holocene sea level rise on the evolution of the southeastern coast of the Canadian Beaufort Sea. Journal of Coastal Research, 11(2), 494–507.

Héquette, A. & Barnes, P.W. (1990). Coastal retreat and shoreface profile variations in the Canadian Beaufort Sea. Marine Geology, 91(1-2), 113–132.

Hill, P.R., Barnes, P.W., Héquette, A. & Ruz, M.-H. (1994). Arctic coastal shorelines *in* Carter, R.W.G. & Woodroffe, C.D. (eds): Coastal evolution – Late Quaternary shoreline morphodynamics (p. 539). Cambridge, UK.

Hill, P.R., Blasco, S.M., Harper, J.R., & Fissel, D.B. (1991). Sedimentation on the Canadian Beaufort shelf. Continental Shelf Research, 11, 821–842.

Hinzman, L.D., Bettez, N.D., Bolton, W.R., Chapin, F.S., Dyurgerov, M.B., Fastie, C.L., Griffith, B., Hollister, R.D., Hope, A., Huntington, H.P., Jensen, A.M., Jia, G.J., Jorgenson, T., Kane, D.L., Klein, D.R., Kofinas, G., Lynch, A.H., Lloyd, A.H., McGuire, A.D., Nelson, F.E., Oechel, W.C., Osterkamp, T.E., Racine, C.H., Romanovsky, V.E., Stone, R.S., Stow, D.A., Sturm, M., Tweedie, C.E., Vourlitis, G.L., Walker, M.D., Walker, D.A., Webber, P.J., Welker, J.M., Winker, K.S. & Yoshikawa, K. (2005). Evidence and implications of recent climate change in northern Alaska and other arctic regions. Climatic Change, 72(3), 251–298.

Holland, M.M., Bitz, C.M., & Tremblay, B. (2006). Future abrupt reductions in the summer Arctic sea ice. Geophysical Research Letters, 33(23), L23503.

Hoque, M.A., & Pollard, W.H. (2009). Arctic coastal retreat through block failure. Canadian Geotechnical Journal, 46(10), 1103–1115.

Hudak, D.R., & Young, J.M.C. (2002). Storm climatology of the southern Beaufort Sea. Atmosphere-Ocean, 40(2), 145–158.

IPCC. (2007). Climate Change 2007: Synthesis Report (p. 73). Cambridge, UK.

Johannessen, O.M., Bengtsson, L., Miles, M.W., Kuzmina, S.I., Semenov, V.A., Alekseev, G.V., Zakharov, V.F., Bobylev, L.P., Pettersson, L.H., Hasselmann, K. & Cattle, H.P. (2004). Arctic climate change: observed and modeled temperature and sea-ice variability. Tellus, 56A, 328–341.

Jones, B.M., Arp, C.D., Jorgenson, M.T., Hinkel, K.M., Schmutz, J.A., & Flint, P.L. (2009). Increase in the rate and uniformity of coastline erosion in Arctic Alaska. Geophysical Research Letters, 36(3), L03503.

Jones, B.M., Hinkel, K. M., Arp, C. D., & Eisner, W. R. (2008). Modern erosion rates and loss of coastal features and sites, Beaufort Sea coastline, Alaska. Arctic, 61(4), 361–372.

Jones, B.M., Arp, C.D., Beck, R., Grosse, G., Webster, J.M., & Urban, F.E. (2009). Erosional history of Cape Halkett and contemporary monitoring of bluff retreat, Beaufort Sea coast, Alaska. Polar Geography, 32(3-4), 129–142.

Jorgenson, M.T. and Brown, J. (2005). Classification of the Alaskan Beaufort Sea coast and estimation of carbon and sediment inputs from coastal erosion. Geo-Marine Letters, 25(2-3), 69–80.

Kobayashi, N., Vidrine, J.C., Nairn, R.B., & Solomon, S.M. (1999). Erosion of frozen cliffs due to storm surge on Beaufort Sea coast. Journal of Coastal Research, 15(2), 332–344.

Kobayashi, N. (1985). Formation of thermoerosional niches into frozen bluffs due to storm surges on the Beaufort Sea coast. Journal of Geophysical Research, 90(C6), 983–988.

Lackenbauer, W.P., Farish, M.J., & Arthur-Lackenbauer, J. (2005). The Distant Early Warning (DEW) Line: A bibliography and documentary resource list (p. 122). Arctic Institute of North America.

Lambert, S.J. (1995). The effect of enhanced greenhouse warming on winter cyclone frequencies and strengths. Journal of Climate, 8, 1447–1452.

Lantuit, H., & Pollard, W.H. (2008). Fifty years of coastal erosion and retrogressive thaw slump activity on Herschel Island, southern Beaufort Sea, Yukon Territory, Canada. Geomorphology, 95(1-2), 84–102.

Lantuit, H., Overduin, P.P., & Couture, N.J. (2008). Sensitivity of coastal erosion to ground ice contents: An Arctic-wide study based on the ACD classification of arctic coasts. Conference Proceedings to the Ninth International Conference of Permafrost. University of Alaska Fairbanks.

Lantuit, H., Overduin, P.P., Couture, N.J., Wetterich, S., Aré, F., Atkinson, D., Brown, J., Cherkashov, G., Drozdov, D., Forbes, D.L., Graves-Gaylord, A., Grigoriev, M., Hubberten, H.-W., Jordan, J., Jorgenson, T., Ødegård, R.S., Ogorodov, S., Pollard, W.H., Rachold, V., Sedenko, S., Solomon, S.M., Steenhuisen, F., Streletskaya, I. & Vasiliev, A. (2011). The Arctic Coastal Dynamics Database: A new classification scheme and statistics on arctic permafrost coastlines. Estuaries and Coasts, 1–18.

Lewellen, R.I. (1973). The occurrence and characteristics of nearshore permafrost, northern Alaska in Permafrost. North American contribution to the second international conference. Yakutsk, Russia.

Lewis, C.P. & Forbes, D.L. (1974): Sediments and sedimentary processes, Yukon Beaufort Sea coast. Environmental-Social Committee, Northern Pipelines, Report.

MacKay, J.R. (2000). Thermally induced movements in ice-wedge polygons, western arctic coast: a long-term study. Géographie physique et Quaternaire, 54(1), 41.

McDonald, B.C. and Lewis, C.P. (1973): Geomorphic and sedimentologic processes of rivers and coasts, Yukon coastal Plain. Environmental-Social Committee, Northern Pipelines, Report, 73-39.

Manson, G.K., & Solomon, S.M. (2007). Past and future forcing of Beaufort Sea coastal change. Atmosphere-Ocean, 45(2), 107–122.

Mapsof, 2012: Outline map, Canada. <http://mapsof.net/>. (accessed: 14 Mar 2012).

Mars, J.C., & Houseknecht, D.W. (2007). Quantitative remote sensing study indicates doubling of coastal erosion rate in past 50 yr along a segment of the Arctic coast of Alaska. Geology, 35(7), 583–586.

McGuire, D.A., Anderson, L.G., Christensen, T.R., Dallimore, S., Guo, L., Hayes, J.D., Heimann, M., Lorenson, T.D., MacDonald, R.W. & Roulet, Z. (2009). Sensitivity of the carbon cycle in the Arctic to climate change. Ecological Monographs, 79(4), 523–555.

McGuire, D.A., Melillo, J.M., Kicklighter, D.W., & Joyce, L.A. (1995). Equilibrium responses of soil carbon to climate change. Journal of Biogeography, 22, 785–796.

Meehl, G.A., Stocker, T.F., Collins, W.D., Friedlingstein, P., Gaye, A.T., Gregory, J.M., Kitoh, A., Knutti, R., Murphy, J.M., Noda, A., Raper, S.C.B., Watterson, I.G., Weaver, A.J. & Zhao, Z.-C. (2007). Global climate projections. Climate Change 2007: the physical science basis (pp. 748–845). Cambridge, UK, New York, USA.

Moore, L.J. (2000). Shoreline mapping techniques. Journal of Coastal Research, 16(1), 111–124.

Moore, M. (2011). DEW line history- stations. <http://dewlinehistory.com/stations/> (accessed: 13. Mar 2013).

Mysak, L.A., & Manak, D.K. (1988). Arctic sea ice extent and anomalies, 1953-1984. Climate Research Group Report no. 88-8. McGill University, Montreal.

NAPL (National Air Photo Library) (2010). NAPL On-Line. <http://www.nrcan.gc.ca/earth-sciences/productsservices/
satellite-photography-imagery/aerial-photos/search-air-photos/890> (accessed: 20. Feb 2013).

NAPL (2007). Aerial photography in Canada – a brief history. <http://www.nrcan.gc.ca/earth-sciences/products-services/satellite-photographyimagery/
aerial-photos/about-aerial-photography/942> (accessed: 21. Feb 2013).

National Climate Data and Information Archive 2013a: Canadian climate normals 1971- 2000, Komakuk Beach.
<http://climate.weatheroffice.gc.ca/climate_normals/results_e.html?stnID=1568&prov=&lang=e&dCode=5&dispBack=1&StationName=Komakuk&SearchType=Contains&province=ALL&provBut=&month1=0&month2=12> (accessed: 19. Mar 2013).

National Climate Data and Information Archive 2013b: Daily data report for August 2012 Komakuk Beach.
<http://climate.weatheroffice.gc.ca/climateData/dailydata_e.html?timeframe=2&Prov=YT&StationID=10822&dlyRange=1994-12-30|2013-03-
17&cmdB2=Go&cmdB1=Go&Month=8&Year=2012&cmdB2=Go> (accessed: 19. Mar 2013).

Norris, D. (1975). Geology Herschel Island and Demarcation Point. Map 1514A. Geological Survey of Canada.

NRCan (Natural Resources Canada) (2009). How to do a GPS survey to centimeter accuracy? <http://www.geod.nrcan.gc.ca/edu/rtk_e.php> (accessed: 18. Feb 2013).

NRCan (2008). Geometric distortion in imagery. <http://www.nrcan.gc.ca/earthsciences/
geography-boundary/remote-sensing/fundamentals/2309> (accessed: 21. Feb 2013).

Ogorodov, S. (2003). The role of sea ice in the coastal zone dynamics of the arctic seas. Water Resources, 30(5), 555–564.

Paine, D.P., & Kiser, J.D. (2012). Aerial photography and image interpretation (p. 629). 3rd edition. New Jersey, USA.

PC (Parks Canada) 2009: Komakuk Beach clean-up monitoring. <http://www.pc.gc.ca/docs/v-g/rsrm2003/sec8.aspx> (accessed: 13. Mar 2013).

Perovich, D., Meier, W., Tschudi, M., Gerland, S., & Richter-Menge, J. (2012). NOAA Arctic report card 2012 – sea ice. <http://www.arctic.noaa.gov/reportcard/sea_ice.html> (accessed: 27. Mar 2013).
Ping, C.-L., Michaelson, G.J., Guo, L., Jorgenson, M.T., Kanevskiy, M., Shur, Y., Dou, F. & Liang, J. (2011). Soil carbon and material fluxes across the eroding Alaska Beaufort Sea coastline. Journal of Geophysical Research, 116(G02), 1–12.

Rachold, V., Aré, F., Atkinson, D., Cherkashov, G., & Solomon, S.M. (2004). Arctic Coastal Dynamics (ACD): an introduction. Geo-Marine Letters, 25(2-3), 63–68.

Rachold, V., Grigoriev, M.N., Aré, F., Solomon, S.M., Reimnitz, E., Kassens, H., & Antonow, M. (2000). Coastal erosion vs riverine sediment discharge in the Arctic shelf seas. International Journal of Earth Sciences, 89(3), 450–460.

Rachold, V., Eicken, H., Gordeev, V.V., Grigoriev, M.N., Hubberten, H.-W., Lisitzin,A.P., Shevchenko, V.P. & Schirrmeister, L. (2004). Modern terrigenous organic carbon input to the Arctic Ocean (33–54) *in* Stein, R. & Macdonald, R.W. (Eds.): The organic carbon cycle in the Arctic Ocean (p. 363). Heidelberg, Germany.

Rampton, V.N.. (1982). Quaternary geology of the Yukon Coastal Plain. Geological Survey of Canada, Bulletin 317 (49 p.). Québec, Canada.

Ravens, T.M., Jones, B.M., Zhang, J., Arp, C.D., & Schmutz, J.A. (2012). Process based coastal erosion modeling for Drew Point, North Slope, Alaska. 122–130.

Reimnitz, E., & Aré, F. (1998). Coastal bluff and shoreface comparison over 34 years indicates large supply of erosion products to Arctic seas. Polarforschung, 68, 231–235.

Reimnitz, E., Graves, S.M., & Barnes, P.W. (1988). Beaufort Sea coastal erosion, sediment flux, shoreline evolution, and the erosional shelf profile. U.S. Geological Survey, to accompany map I-1182-G.

Reimnitz, E., & Maurer, D.K. (1979). Effects of storm surges on the Beaufort Sea coast, Northern Alaska. Arctic, 32(4), 329–344.

Reimnitz, E., Barnes, P.W., & Harper, J.R. (1990). A review of beach nourishment from ice transport of shoreface materials, Beaufort Sea, Alaska. Journal of Coastal Research, 6(2), 439–470.

Reimnitz, E., Graves, S.M., & Barnes, P.W. (1985). Beaufort sea coastal erosion, shoreline evolution and sediment flux. U.S. Geological Survey Open File Report 85-380. (p. 67).

Romanovsky, V.E., Smith, S.L., Christiansesn, H.H., Shiklomanov, N.I., Streletskiy, D.A., Drozdov, D.S., Oberman, N.G., Kholodov, A.L. & Marchenko, S.S. (2012). NOAA Arctic report chart 2012 – permafrost. <http://www.arctic.noaa.gov/reportcard/permafrost.html> (accessed: 27. Mar 2013).

Sabatini, R., & Plamerini, G. B. (2008). Differential GPS. Differential Global Positioning System (DGPS) for flight testing. NATO Science and Technology Organization. (pp.1–18).

Schwartz, M.L. (Ed.). (2005). Encyclopedia of Coastal Science (p. 1211). Washington, USA.

Serreze, M.C, Walsh, J.E., Osterkamp, T., Dyurgerov, M., Romanovsky, V., Oechel, W.C., Morison, J., Zhang, T. & Barry, R.G. (2000). Observational evidence of recent change in the northern high-latitude environment. Climate Change, 46, 159–207.

Serreze, M.C., & Francis, J. (2006). The Arctic amplification debate. Climatic Change, 76(3-4), 241–264.

Solomon, S.M., & Gareau, P. (2003). Beaufort Sea coastal mapping and the development of an erosion hazard index. Proceedings of the eight International Conference on Permafrost. Zurich, Swiss.

Solomon, S.M. (1998). Draft report to Department of National Defence and Ivvavik National Park on coastal erosion at the Komakuk DEW Line site. Unpublished (p. 15).

Solomon, S.M. (2005). Spatial and temporal variability of shoreline change in the Beaufort-Mackenzie region, Northwest Territories, Canada. Geo-Marine Letters, 25(2-3), 127–137.

Solomon, S.M., Forbes, D.L., & Kierstead, B. (1994). Coastal impacts of climate change: Beaufort sea erosion study. Geological Survey of Canada Open File Report 2890. (p. 35).

TAGA (Toolik-Arctic Geobotanical Atlas) 2013: Glossary - Tussock tundra. <http://www.arcticatlas.org/glossary/#T> (access: 19. Mar 2013).

Tarnocai, C., Canadell, J.G., Schuur, E.A.G., Kuhry, P., Mazhitova, G., & Zimov, S. (2009). Soil organic carbon pools in the northern circumpolar permafrost region. Global Biogeochemical Cycles, 23(2), 1–11.

Thieler, E.R., Himmelstoss, E.A., Zichichi, J.L., & Ayhan, E. (2009). Digital Shoreline Analysis System (DSAS) version 4.0 - An ArcGIS extension for calculating shoreline change: U.S. Geological Survey Open-File Report 2008-1278. Updated for version 4.3. (p. 79).

Treut, L., Somerville, R., Cubasch, U., Ding, Y., Mauritzen, C., Mokssit, A., Peterson, T. & Parther, M. (2007). Historical overview of climate change science (93-127) *in* Solomon, S. M., Qin, D., Manning, M., Chen, Z., Marquis, M., Averyt, K. B., Tingor, M. & Miller, H. L. (eds.): Climate Change 2007: The Physical Science Basis. Contribution of Working Group I to the Fourth Assessment Report of the Intergovernmental Panel on Climate Change. Cambridge, UK, New York, USA.

Vonk, J.E., Sánchez-García, L., Van Dongen, B.E., Alling, V., Kosmach, D., Charkin, A., Semiletov, I. P., Dudarev, O.V., Shakhova, N., Roos, P., Eglinton, T.I., Anderson, A. & Gustafsson, Ö. (2012). Activation of old carbon by erosion of coastal and subsea permafrost in Arctic Siberia. Nature, 489(7414), 137–40.

Welsh, S.L., & Rigby, K. (1971). Botanical and physiographic reconnaissance. Birgham Young University Science Bulletin, XIV(2), 64.

Zhang, Y., & Chen, W. (2005). Soil temperature in Canada during the twentieth century: complex responses to atmospheric climate change. Journal of Geophysical Research, 110(D3), 1–15.

Zinas, N. (2011). RTK Phase Positioning. GPS network Real Time Kinematic tutorial. <http://tekmon.gr/research-development/gps-network-rtk-tutorial/> (access: 18 Mar 2013).

Appendices

Appendix I: Southern Beaufort Sea Coast
Appendix II: Air photo management list
Appendix III: Scatter plots for the Border site
Appendix IV: Scatter plots for Komakuk site
Appendix V: Map 1: DSAS results for the whole study area
Appendix VI: Map 2: DSAS analysis results for the Border site
Appendix VII: Map 3: DSAS analysis results for the Komakuk site

Appendix I

Appendix I: Southern Beaufort Sea coast. Study area is indicated with solid line. Points show locations of further coastal change study sites (Table 1). Source: GoogleMaps

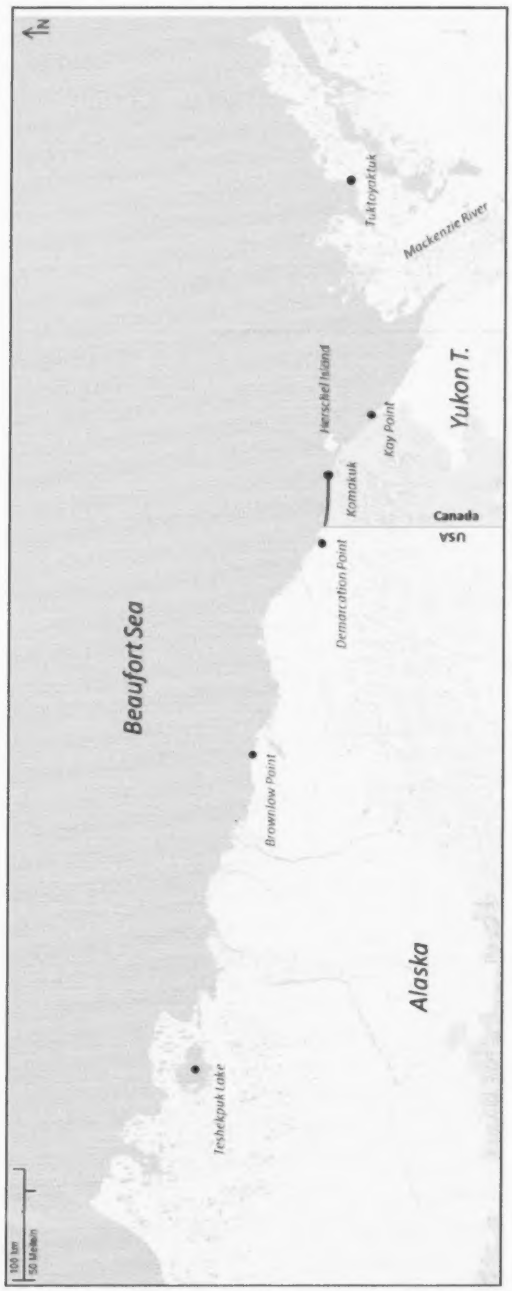

Appendix II

Appendix II: Air photo management list

Date acquired (dd/mm/yyyy)	Roll no.	Photo no.	Scale (1:)	Scanned (dpi)	Pixel resolution [m]	Georeferenced to	Mosaic file name	No. of GCPs	RMS	RMS of Mosaic
7/14/1951	A13140	110	70000	2400	0.74	SPOT image	Mosaic_1951_All	30	3.38	2.63
7/14/1951	A13231	69	70000	1800	0.99	SPOT image		32	3.46	
7/14/1951	A13231	67	70000	1800	0.99	SPOT image		37	3.91	
7/14/1951	A13138	154	70000	1800	0.99	SPOT image		41	3.78	
7/18/1964	VRR2613	53	5000	600	0.21	Mosaic_1975	Mosaic_1964_Kom	21	0.70	0.73
7/18/1964	VRR2613	54	5000	600	0.21	Mosaic_1975		39	0.84	
7/18/1964	VRR2613	55	5000	600	0.21	Mosaic_1975		26	0.65	
7/8/1972	A22879	2	60000	2000	0.76	Mosaic_1964	Mosaic_1972_All	28	2.90	2.58
7/8/1972	A22879	100	60000	2000	0.76	Mosaic_1951		40	2.71	
7/8/1972	A22879	20	60000	2000	0.76	Mosaic_1951		29	2.84	

7/9/1972	A22881	112	60000	600	2.54	Mosaic_1951		20	1.79	
6/27/1975	A24089	49	5000	600	0.21	Mosaic_1984	Mosaic_1975_Kom	31	0.57	0.47
6/27/1975	A24089	50	5000	600	0.21	Mosaic_1984		25	0.40	
6/27/1975	A24089	51	5000	600	0.21	Mosaic_1984		23	0.40	
6/27/1975	A24089	52	5000	600	0.21	Mosaic_1984		27	0.53	
7/7/1976	A24502	3	60000	2000	0.76	Mosaic_1951	Mosaic_1976_Bor	32	1.65	1.65
9/1/1984	A26598	36	5000	600	0.21	Mosaic_1992	Mosaic_1984_Kom	24	0.48	0.52
9/1/1984	A26598	37	5000	600	0.21	Mosaic_1992		25	0.45	
9/1/1984	A26598	38	5000	600	0.21	Mosaic_1992		29	0.44	
9/1/1984	A26598	39	5000	600	0.21	Mosaic_1992		18	0.36	
8/6/1992	A28263	102	6000	600	0.25	Mosaic_1993	Mosaic_1992_Kom	24	0.44	0.57

8/6/1992	A28263	103	6000	600	0.25	Mosaic_1993		26	0.73	
8/6/1992	A28263	104	6000	600	0.25	Mosaic_1993		26	0.64	
8/6/1992	A28263	105	6000	600	0.25	Mosaic_1993		40	0.62	
8/6/1992	A28263	106	6000	600	0.25	Mosaic_1993		26	0.43	
8/6/1992	A28263	107	6000	600	0.25	Mosaic_1993		27	0.44	
8/6/1992	A28263	108	6000	600	0.25	Mosaic_1993		28	0.68	
8/6/1992	A28263	113	6000	600	0.25	Mosaic_1972	Mosaic_1992_Bor	19	0.68	0.75
8/6/1992	A28263	114	6000	600	0.25	Mosaic_1972		24	0.83	
8/6/1992	A28263	115	6000	600	0.25	Mosaic_1972		17	0.48	
8/6/1992	A28263	116	6000	600	0.25	Mosaic_1994		28	0.81	
8/6/1992	A28263	117	6000	600	0.25	Mosaic_1994		21	0.85	
8/6/1992	A28263	118	6000	600	0.25	Mosaic_1994		19	0.77	

8/6/1992	A28263	119	6000	600	0.25	Mosaic_1994		25	0.80	
7/8/1993	A28001	109	20000	1200	0.42	SPOT image	Mosaic_1993_Kom	31	1.94	2.13
7/8/1993	A28001	110	20000	1200	0.42	SPOT image		30	2.68	
7/8/1993	A28001	111	20000	1200	0.42	SPOT image		40	1.77	
7/13/1994	A28126	70	6000	600	0.25	Mosaic_1951	Mosaic_1994_Bor	23	0.96	1.03
7/13/1994	A28126	71	6000	600	0.25	Mosaic_1951		27	1.12	
7/13/1994	A28126	72	6000	600	0.25	Mosaic_1951		49	1.32	
7/13/1994	A28126	73	6000	600	0.25	Mosaic_1951		26	1.02	
7/13/1994	A28126	74	6000	600	0.25	Mosaic_1951		25	1.02	
7/13/1994	A28126	75	6000	600	0.25	Mosaic_1951		26	0.92	
7/13/1994	A28126	76	6000	600	0.25	Mosaic_1951		24	0.88	

Appendix III

Appendix III: Scatter plots with linear regression line for each shore profile parameter at the Border site

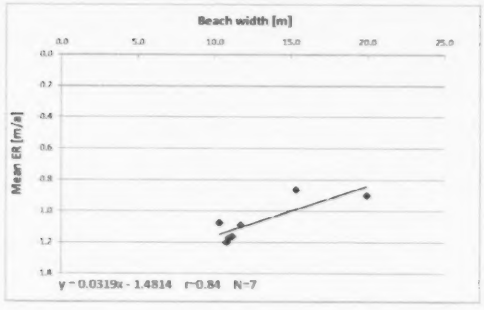

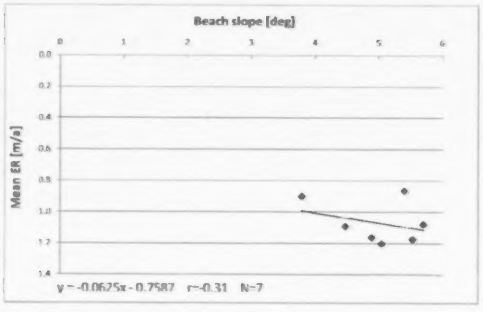

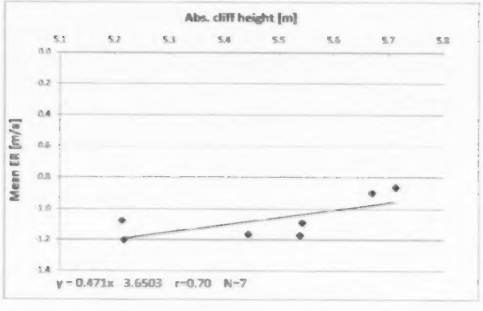

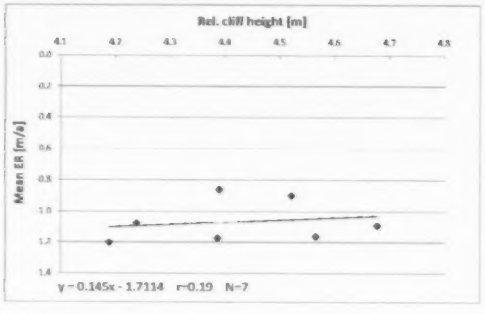

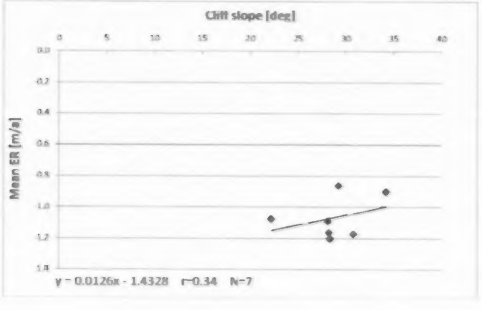

Appendix IV

Appendix IV: Scatter plots with linear regression line for each shore profile parameter at the Komakuk site

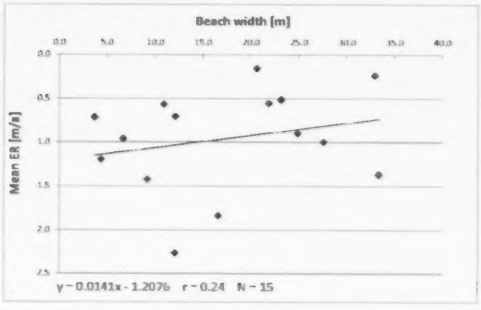

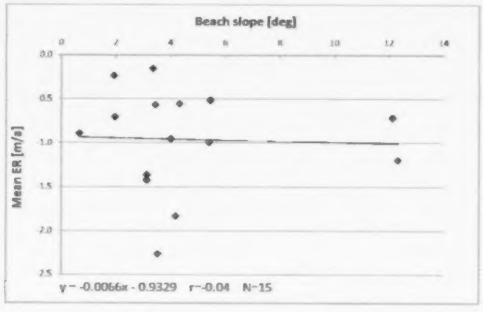

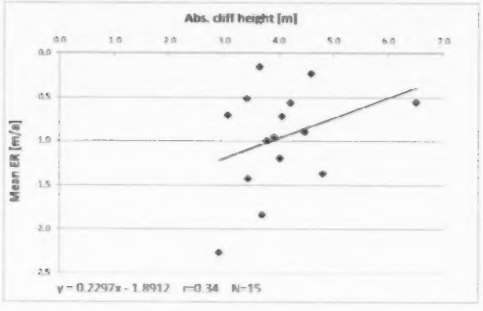

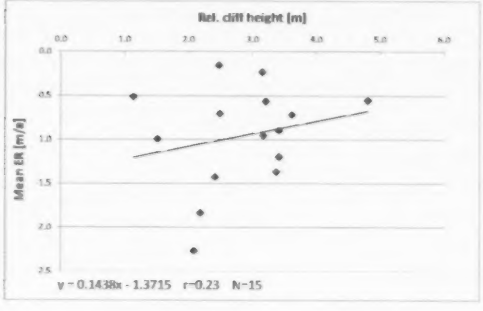

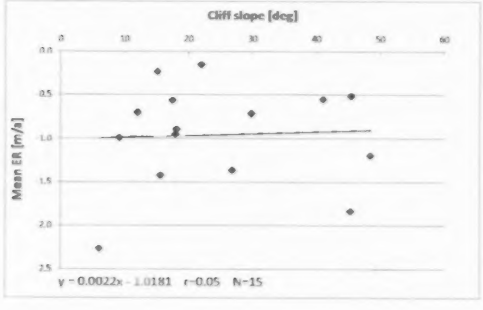

Appendix V:

Map 1: DSAS analysis results for the whole study area

Coastal change within the last 58 years along the western Yukon coast, Canada

Rate of change [m/a]

- -2.85 to -2.00
- -1.99 to -1.50
- -1.49 to -1.00
- -0.99 to -0.50
- -0.49 to 0.76

Shoreline change statistics were computed with Esri ArcGIS extension DSAS v. 4.3, based on 50 m transect spacing.

Rates of change are end point rate values. Each transect value is assigned to the polygon to its right.

Shorelines

- 1951
- 1972
- 2009

International border

Cartography: A.M. Konopczak,Christian-Albrechts Universität zu Kiel, in cooperation with Geological Survey of Canada, Atlantic.

April, 2013

Appendix VI

Map 2: DSAS analysis results for the Border site

MAP 2 DSAS analysis results for the Border site

Appendix VII

Map 3: DSAS analysis results for the Komakuk site

MAP 3 DSAS analysis results for the Komakuk site